New Closed Form Analysis of Resonances in Microwave Power for Material Processing

Madhuchhanda Bhattacharya
Dept. of Chemical Engineering, Central Leather Research Institute, Adyar, Chennai 600 020, India

Tanmay Basak
Dept. of Chemical Engineering, Indian Institute of Technology, Madras, Chennai 600 036, India

DOI 10.1002/aic.10979
Published online October 2, 2006 in Wiley InterScience (www.interscience.wiley.com).

A new closed form material invariant analysis on resonances of microwave induced power absorption is presented. It is shown that resonances in average power is confined within two asymptotic limits of thin and thick samples, and the resonances occur if $\lambda_m \leqslant 1.5D_{p,m}$ *for* $\lambda_m \approx \lambda_0$ *and* $\lambda_m \leqslant 3D_{p,m}$ *for* $\lambda_m \not\approx \lambda_0$. *Here* λ_m *and* $D_{p,m}$ *denote the wavelength and penetration depth within the sample, respectively, and* λ_0 *is the wavelength within the free space. It has been shown that average absorbed power does not exhibit resonance for one side incidence if* $\lambda_m \approx \lambda_0$, *while the occurrence of resonance is independent of* ϕ_l *for* $\lambda_m \not\approx \lambda_0$. *Here,* ϕ_l *is the fractional power input from the left side. The amplitudes of subsequent resonating peaks are also shown to decay monotonically with sample length for* $\lambda_m \approx \lambda_0$, *while they vary nonmonotonically for* $\lambda_m \not\approx \lambda_0$ *and* $\phi_l \not\approx 0, 1$ *or* 1/2 *due to suppressions of odd (for* $\lambda_m < \lambda_0$), *or even (for* $\lambda_m > \lambda_0$) *resonating peaks, which increase as* ϕ_l *approaches* 1/2 *from either* 0 *or* 1. *Finally, at* $\phi_l \approx 1/2$ *with* $\lambda_m \not\approx \lambda_0$ *odd (for* $\lambda_m < \lambda_0$), *or even (for* $\lambda_m > \lambda_0$) *resonating peaks of average absorbed power vanish reducing the number of resonating points by a factor of two from one side incidence (*$\phi_l \approx 0$ *or* 1), *to both side incidence with equal power input from left and right sides (*$\phi_l \approx 1/2$). *This work provides correlations (corresponding to* $\lambda_m \approx \lambda_0$ *and* $\lambda_m \not\approx \lambda_0$) *for predicting the locations of resonating peaks as function of* λ_m/λ_0, $\lambda_m/D_{p,m}$, *and* ϕ_l. *The theoretical prediction on average power characteristics have been shown to be useful in forecasting the heating patterns for efficient material processing.* © 2006 American Institute of Chemical Engineers *AIChE J,* 52: 3707–3721, 2006
Keywords: microwave, power, closed form, resonances

Introduction

Presence of maxima in microwave induced absorbed power vs. sample dimension was first reported in experimental work on cylinders and spheres (Ohlsson and Risman, 1978; Massoudi et al., 1979; Weil, 1975), which was further supported by theoretical investigations on one-dimensional (1-D) slabs, and 2-D cylinders (Ayappa et al., 1991; Ayappa et al., 1992; Ayappa et al., 1997; Ayappa, 1999; Barringer et al., 1995; Basak and Priya, 2005). Based on numerical studies for some specific materials (for example, oil, water, potato, beef, and so on), earlier researchers concluded that wavelength within the sample (denoted by λ_m in the text) is the only factor governing the nonmonotonicity of absorbed power (Ayappa et al., 1991; Ayappa et al., 1992; Ayappa et al., 1997; Ayappa, 1999; Barringer et al., 1995; Basak and Priya, 2005). Later, material invariant numerical analysis by Basak and Kumaran (2005), and Basak (2005), revealed that penetration depth within the

Correspondence concerning this article should be addressed to T. Basak at tanmay@iitm.ac.in

sample (denoted by $D_{p,m}$), as well as wavelength within free space (denoted by λ_0) are additional factors which influence the resonance of maxima of absorbed power. However, due to the lack of proper closed form solution, exact characterization of nonmonotonic features of absorbed power could not be established in the literature.

This work fills the gap by providing a close form solution and quantifying various resonating characteristics of average absorbed power in a 1-D slab exposed to microwave radiations of various intensities from left and right sides. A detailed analysis of this analytical form of average absorbed power has been carried out to study the resonating characteristics confined within two asymptotic limits of thick and thin samples. The average power within the resonating regime, as well as thin and thick sample limits has been investigated with respect to various factors, such as the wavelengths, penetration depth, and the distribution of microwave sources. We have provided various relations for predicting resonating sample lengths as functions of λ_m, $D_{p,m}$, λ_0, and the distribution of microwave source. These formula clearly illustrate that the correlation developed by earlier researchers (Ayappa et al., 1997; Ayappa, 1999) is a subset of the relations reported in this work, which results in the limit of $\lambda_m \ll 2\pi D_{p,m}$. Moreover, all of the earlier work are limited to either one-side incidence, or both-side incidence, with equal power input from left and right sides. As a result, previous workers overlooked some of the inherent characteristics of resonating features of average absorbed power. This article initiates a first attempt to illustrate the influence of both-side incidence, with various distributions of microwave power input from left and right sides, as well as the ratios λ_0/λ_m, $D_{p,m}/\lambda_m$ revealing a strong functionality between the resonating patterns of average absorbed power and the aforementioned factors.

The theoretical investigations are further analyzed for processing of various food and ceramic materials. The average power characteristics for various regimes have been shown to have one to one correspondence with spatial and global heating patterns. Final recommendation on efficient heating policy has been discussed based on the theoretical analysis.

Electric Field and Power Distributions

Uniform plane microwave induced electric field ($E_{x,m}$), and absorbed power ($q(z')$) within a 1-D sample (as shown in Figure 1) obey the following relation

$$q(z') = \pi f \varepsilon_0 \kappa''_m E_{x,m}(z') E^*_{x,m}(z') \tag{1}$$

with $E_{x,m}$ satisfying the Helmholtz equation (Stratton, 1941; Balanis, 1989) given by

$$\frac{d^2E_{x,m}}{dz'^2} + \kappa_m^2 E_{x,m} = 0, \quad z' \in \{-L, L\} \tag{2}$$

In Eq. 1, superscript "*" denotes complex conjugate, f is the frequency of radiation, ε_0 is the free space permittivity, and κ_m represents the propagation constant of the sample defined as

$$\kappa_m = \frac{2\pi f}{c} \sqrt{\kappa'_m + i\kappa''_m} \tag{3}$$

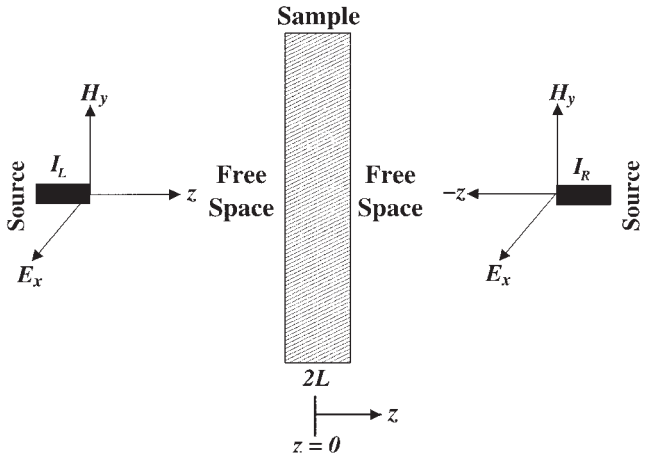

Figure 1. 1-D sample exposed to plane electromagnetic radiations from left and right sides.

with κ'_m and κ''_m as dielectric constant and dielectric loss, respectively, and c as the velocity of light. κ_m can also be written in terms of wavelength (λ_m) and penetration depth ($D_{p,m}$) within the sample as

$$\kappa_m = \frac{2\pi}{\lambda_m} + i\,\frac{1}{D_{p,m}} \tag{4}$$

where

$$\lambda_m = \frac{c\sqrt{2}}{f\left[\sqrt{(\kappa'_m)^2 + (\kappa''_m)^2} + \kappa'_m\right]^{1/2}} \tag{5a}$$

and

$$D_{p,m} = \frac{c}{\sqrt{2}\,\pi f\left[\sqrt{(\kappa'_m)^2 + (\kappa''_m)^2} - \kappa'_m\right]^{1/2}} \tag{5b}$$

Considering propagation of electromagnetic wave through the surrounding free space, determination of $E_{x,m}$ requires the solution of following coupled equations

$$\frac{d^2E_{x,j}}{dz'^2} + \kappa_j^2 E_{x,j} = 0, \quad j = \begin{cases} l & z' < -L \\ m & -L \leq z' \leq L \\ r & z' > L \end{cases} \tag{6}$$

with

$$\left.\begin{aligned} E_{x,l} &= E_{x,m} \\ \frac{dE_{x,l}}{dz'} &= \frac{dE_{x,m}}{dz'} \end{aligned}\right\} \text{at } z' = -L \text{ and } \left.\begin{aligned} E_{x,m} &= E_{x,r} \\ \frac{dE_{x,m}}{dz'} &= \frac{dE_{x,r}}{dz'} \end{aligned}\right\} \text{at } z' = L \tag{7}$$

where subscripts l and r denote left and right side free space, respectively, and symbols $E_{x,j}$ and κ_j, $j = l, r$ represent the corresponding free space variables. It may be noted that propagation constant is in general a complex number, except for free space, which has zero dielectric loss and dielectric constant as unity (that is, $\kappa_j' = 1$ and $\kappa_j'' = 0$, $j = l, r$). In free space, incident flux of radiation (I_0) is related to electric field intensity (E_0) by

$$E_0 = \sqrt{\frac{2I_0}{c\varepsilon_0}} \tag{8}$$

Thus, for both-side incidence with I_L and I_R as flux of radiation from left and right side, respectively, (refer to Figure 1), incident electric field intensities from left (E_L), and right (E_R) sides are given by

$$E_L = \sqrt{\frac{2I_L}{c\varepsilon_0}}, \quad E_R = \sqrt{\frac{2I_R}{c\varepsilon_0}} \tag{9}$$

Solution of Eq. 6 can be written as a combination of transmitted and reflected waves

$$E_{x,j} = E_{1,j}e^{i\kappa_j z'} + E_{2,j}e^{-i\kappa_j z'}, \quad j = l, m, r \tag{10}$$

where $E_{1,j}$ and $E_{2,j}$ are transmission and reflection coefficients, respectively, with

$$E_{1,l} = E_L \text{ and } E_{2,r} = E_R \tag{11}$$

Other coefficients ($E_{2,l}$, $E_{1,m}$, $E_{2,m}$, $E_{1,r}$) can be uniquely determined by using Eq. 7, which results in the following expression for $E_{x,m}$

$$E_{x,m} = E_T \frac{\sum_{k=l}^{r} 2\kappa_k e^{-i\kappa_k L}(\kappa_m \cos \kappa_m L(1+\sigma z) - i\kappa_j \sin \kappa_m L(1+\sigma z))\phi_k}{\kappa_m(\kappa_l + \kappa_r)\cos 2\kappa_m L - i(\kappa_m^2 + \kappa_l\kappa_r)\sin 2\kappa_m L} \tag{12}$$

where $\sigma = 1, -1$, and $j = l, r$ for $k = r, l$, respectively, $E_T = E_L + E_R$, and dimensionless variables ϕ_l, ϕ_r, and z are given by

$$z = \frac{z'}{L}, \quad \phi_l = \frac{E_L}{E_L + E_R}, \quad \phi_r = \frac{E_R}{E_L + E_R} \equiv 1 - \phi_l \tag{13}$$

It may be noted that $0 \leq \phi_l \leq 1$ and $0 \leq \phi_r \leq 1$ are fractional incident electric fields from left and right-side, respectively. Here, $\phi_l = 0$ or $\phi_r = 1$ (right-side) and $\phi_l = 1$ or $\phi_r = 0$ (left side) correspond to one side incidence, while ϕ_l or $\phi_r \neq 0$ or 1 represent both-side incidence. For $\phi_l = \phi_r = 1/2$, the intensities of radiations from left and right-sides are same, while they are different for ϕ_l or $\phi_r \neq 1/2$. As Eq. 9 is valid only for free space, Eq. 12 with I_L or $I_R \neq 0$ (that is, both-side incidence) is limited to $\kappa_l = \kappa_r = \kappa_0$, where $\kappa_0 = 2\pi/\lambda_0$ is the propagation constant of free space with $\kappa_0' = 1$, $\kappa_0'' = 0$, and $\lambda_0 = f/c$ is the wavelength within free space. However, for one-side incidence, Eq. 12 is still valid for a dummy load with high-dielectric loss (for example, water) on the opposite face of incidence. Therefore, to maintain the generality, we present the solution for $\kappa_j|_{j=l,r} \neq \kappa_0$, and adopt $\kappa_j|_{j=l,r} = \kappa_0$, for both-side incidence.

For the sake of simplicity in algebraic notations, we rewrite the propagation constant as

$$\kappa_j = \kappa_{jR} + i\kappa_{jI}, \quad j = l, m, r \tag{14}$$

where $\kappa_{jR} = 2\pi/\lambda_j$ and $\kappa_{jI} = 1/D_{p,j}$, λ_j, and $D_{p,j}$ being wave length and penetration depth in jth medium, respectively. Then, taking complex conjugate of $E_{x,m}$, the distribution of dimensionless absorbed power may be written as

$$Q(z) = \frac{C_q^l(z)\phi_l^2 + C_q^r(z)\phi_r^2 + 2C_q^{lr}(z)\phi_l\phi_r}{C_q^d} \tag{15}$$

where

$$Q(z) = q(z'/L)/Q_0$$

with

$$Q_0 = \pi f \varepsilon_0 \kappa_m'' E_T^2$$

and

$$C_q^k = c_{q,1}^k \cos(2\kappa_{mR}L(1+\sigma z)) + c_{q,2}^k \cosh(2\kappa_{mI}L(1+\sigma z)) + c_{q,3}^k \sin(2\kappa_{mR}L(1+\sigma z)) + c_{q,4}^k \sinh(2\kappa_{mI}L(1+\sigma z)), \quad k = l, r, \tag{16a}$$

$$C_q^{lr} = c_{q,1}^{lr}\cosh(2\kappa_{mI}Lz) - c_{q,2}^{lr}\sinh(2\kappa_{mI}Lz) + c_{q,3}^{lr}\cos((\kappa_{lR} - \kappa_{rR})L - 2\kappa_{mR}Lz) + c_{q,4}^{lr}\cos((\kappa_{lR} - \kappa_{rR})L + 2\kappa_{mR}Lz) + c_{q,5}^{lr}\sin((\kappa_{lR} - \kappa_{rR})L - 2\kappa_{mR}Lz) - c_{q,6}^{lr}\sin((\kappa_{lR} - \kappa_{rR})L + 2\kappa_{mR}Lz)), \tag{16b}$$

and

$$C_q^d = c_{q,1}^d \cos(4\kappa_{mR}L) + c_{q,2}^d \cosh(4\kappa_{mI}L) + c_{q,3}^d \sin(4\kappa_{mR}L) + c_{q,4}^d \sinh(4\kappa_{mI}L) \tag{16c}$$

with the coefficients $c_{q,j}^k$, $c_{q,j}^{lr}$, and $c_{q,j}^d$ given in Appendix A.

Asymptotes: Thick and Thin sample

It may be noted from Eq. 15 that absorbed power becomes weak function of position if sample length ($2L$) is much smaller than $L_{min} = \min(1/\kappa_{mR}, 1/\kappa_{mI})$, while it decays exponentially within the sample $2L \gg 1/\kappa_{mI}$ or $D_{p,m}$. The first limit is called as *thin* sample, while the later is called as *thick* sample.

In the thin sample limit, nearly uniform power distribution is attained within the sample, where an asymptotic expansion results in the following 4th-order asymptotes for $Q(z)$

$$\lim_{(2L/L_{\min})\ll 1} C_q^k = \sum_{j=0}^{2} \frac{2^{2j}(1+\sigma z)^{2j}}{(2j)!}\left((-1)^j c_{q,1}^k \varepsilon_R^{2j} + c_{q,2}^k \varepsilon_I^{2j}\right) + \sum_{j=0}^{1} \frac{2^{2j+1}(1+\sigma z)^{2j+1}}{(2j+1)!}\left((-1)^j c_{q,3}^k \varepsilon_R^{2j+1} + c_{q,4}^k \varepsilon_I^{2j+1}\right), \quad k = l, r, \tag{17a}$$

$$\lim_{(2L/L_{\min})\ll 1} C_q^{lr} = 4\sum_{j=0}^{4}\left(\chi_j^{lc}\cos(\kappa_{lR}L - \kappa_{rR}L) + (-1)^{j+1}\chi_j^{ls}\sin(\kappa_{lR}L - \kappa_{rR}L)\right)\varepsilon_R^j e^{(\kappa_{lI}+\kappa_{rI})L} \tag{17b}$$

$$\lim_{(2L/L_{\min})\ll 1} C_q^{d} = \sum_{j=0}^{2} \frac{4^{2j}}{(2j)!}\left((-1)^j c_{q,1}^d \varepsilon_R^{2j} + c_{q,2}^d \varepsilon_I^{2j}\right) + \sum_{j=0}^{1} \frac{4^{2j+1}}{(2j+1)!}\left((-1)^j c_{q,3}^d \varepsilon_R^{2j+1} + c_{q,4}^d \varepsilon_I^{2j+1}\right) \tag{17c}$$

with

$$\varepsilon_R = \kappa_{mR}L, \quad \varepsilon_I = \kappa_{mI}L. \quad l_s = \begin{cases} i \text{ for even } j \\ r \text{ for odd } j \end{cases} \qquad l_c = \begin{cases} r \text{ for even } j \\ i \text{ for odd } j \end{cases}. \tag{18}$$

Denoting $\vartheta_{i,j}^{+l} = \vartheta_i^l + \vartheta_j^l$ and $\vartheta_{i,j}^{-l} = \vartheta_i^l - \vartheta_j^l$, the expressions for χ^l, $l = i, r$ can be written as

$$\chi_0^l = \vartheta_1^l + (\vartheta_{2,3}^{+l} + \vartheta_{2,3}^{-l}z)\varepsilon_I + (\vartheta_{1,4}^{+l} + \vartheta_{1,4}^{-l}z^2)\varepsilon_I^2 + \frac{2}{3}(\vartheta_{2,3}^{+l} + \vartheta_{2,3}^{-l}z^3)\varepsilon_I^3 + \frac{1}{3}(\vartheta_{1,4}^{+l} + \vartheta_{1,4}^{-l}z^4)\varepsilon_I^4 \tag{19a}$$

$$\chi_1^l = \vartheta_{2,3}^{-l} + \vartheta_{2,3}^{+l}z + 4\vartheta_1^l\varepsilon_I z + 2(\vartheta_{2,3}^{+l} + \vartheta_{2,3}^{-l}z)\varepsilon_I^2 z + \frac{4}{3}(\vartheta_{1,4}^{+l} + \vartheta_{1,4}^{-l}z^2)\varepsilon_I^3 z \tag{19b}$$

$$\chi_2^l = -\vartheta_{1,4}^{-l} - \vartheta_{1,4}^{+l}z^2 - 2(\vartheta_{2,3}^{-l} + \vartheta_{2,3}^{+l}z)\varepsilon_I z - 4\vartheta_1^l\varepsilon_I^2 z^2 \tag{19c}$$

$$\chi_3^l = -\frac{2}{3}(\vartheta_{2,3}^{-l} + \vartheta_{2,3}^{+l}z^3) - \frac{4}{3}(\vartheta_{1,4}^{-l} + \vartheta_{1,4}^{+l}z^2)\varepsilon_I z \tag{19d}$$

$$\chi_4^l = \frac{1}{3}(\vartheta_{1,4}^{-l} + \vartheta_{1,4}^{+l}z^4) \tag{19e}$$

where ϑ_j^r and ϑ_j^i, $j = 1$–4 are given in Appendix A, with $\vartheta_4^i = 0$. It may be noted that Eqs. 17–19 are based on the assumption that $O(\kappa_{mR}) \sim O(\kappa_{mI})$, and can be further simplified for the case of $\kappa_{mR} \gg \kappa_{mI}$ (or vice versa) by neglecting smaller order terms accordingly.

On the other hand, exponential terms of Eq. 15 dominate over sinusoidal terms for $2L \gg D_{p,m}$, and thick sample asymptotes of $Q(z)$ can be written as

$$Q(z) = 4\sum_{k=l}^{r} \frac{|\kappa_k|^2 e^{2\kappa_{kI}L-(1-\sigma z)2\kappa_{mI}L}\phi_k^2}{|\kappa_k|^2 + |\kappa_m|^2 + 2\delta_{km}^R} \tag{20}$$

where $|\cdot|$ denotes the modulus of a complex quantity. It follows that for the case of both side incidence (ϕ_l or $\phi_r \neq 0$) exponential decay of absorbed power occurs from both sides.

Average Power: Resonance

Integrating Eq. 15 from $z = -1$ to $z = 1$, dimensionless average power (Q_{avg}) can be written as

$$Q_{avg} = \frac{1}{2}\int_{-1}^{1} Q(z)dz = \frac{C_0^n + C_1^n\sin\left(\frac{4\pi L}{\lambda_m} + \eta_{n,1}\right) + C_2^n\sin\left(\frac{8\pi L}{\lambda_m} - \eta_{n,2}\right)}{2\kappa_{mR}L\left[C_0^d + C_1^d\sin\left(\frac{8\pi L}{\lambda_m} + \eta_d\right)\right]} \tag{21}$$

where C_0^n, C_0^d, C_1^n, C_2^n, C_1^d, $\eta_{n,1}$, $\eta_{n,2}$, and η_d are given in Appendix B. It follows that average absorbed power has both exponential and sinusoidal dependencies on sample length, where the later governs nonmonotonic variations of Q_{avg} with L leading to peaks or maxima in Q_{avg} vs. L plot, which will be referred to as *resonance*. It is interesting to note that nonmonotonicity in Q_{avg} may result either from the interactions of electromagnetic wave, with the sample captured by the sine terms in Eq. 21, or from the propagation of two incident electromagnetic waves through two different surrounding mediums on left and right sides of the sample, which is captured by sin γ and cos γ terms in C_1^Q and $\eta_{n,1}$ (refer to Appendix B). It may also be noted that $C_1^n = 0$ for one-side incidence ($\phi_l = 0$ or $\phi_r = 0$), which restricts nonmonotonic features of Q_{avg} due to nonzero γ to both-side incidence. However, as mentioned before, the solutions presented here with ϕ_l or $\phi_r \neq 0$ are valid only for $\kappa_l = \kappa_r = \kappa_0$, which results in $\gamma = 0$. Therefore, Q_{avg} can exhibit nonmonotonicity only due to the sine functions in Eq. 21, and following discussion will be based on the assumption that $\kappa_l = \kappa_r = \kappa_0$.

As can be seen from Eq. 21, nonmonotonic features of Q_{avg} depend on relative contributions from C_0^n, C_1^n, C_2^n, C_0^d, and C_1^d, which in turn depend on relative magnitude of $\kappa_{0R} = \kappa_0$, κ_{mR}, and κ_{mI}. Thus, it is imperative to assign relative orders of magnitude to κ's in order to characterize nonmonotonic features of Q_{avg} in the whole parameter space of $\{\kappa_0, \kappa_{mR}, \kappa_{mI}\}$. Due to κ_{mR}'s primary role in determining the frequency of nonmonotonicity, we assign

$$\kappa_0 = p\kappa_{mR}, \quad \kappa_{mI} = n\kappa_{mR} \tag{22}$$

where $0 \leqslant n \leqslant 1$ according to Eq. 5a and b. This allows us to impose various orders of magnitude to κ's by varying n from 0 to 1, and p from 0 to ∞ mimicking different sample-free space combinations. However, not all p and n result in nonmonotonic Q_{avg} vs. L functionality. Therefore, it is necessary to find the bound on p and n for which Q_{avg} behaves nonmonotonically.

Due to positive exponential dependencies, both C_0^n and C_0^d increase with increasing sample length leading to a predominance over sinusoidal terms for $2L \gg D_{p,m}$, where Q_{avg} decays exponentially with sample length. This confines the upper boundary of nonmonotonic regime within the inner boundary of the thick sample asymptote, which can be considered to be $2L = 1.5D_{p,m}$ for all practical purposes as exponential terms in Eq. 21 dominate for $4\kappa_{mI}L \geqslant 3$. Thus at least one full wave corresponding to either of $S_{n,1}$, $S_{n,2}$, or S_d, where

$$S_{n,1} = C_1^n \sin\left(\frac{4\pi L}{\lambda_m} + \eta_{n,1}\right), \quad S_{n,2} = C_2^n \sin\left(\frac{8\pi L}{\lambda_m} - \eta_{n,2}\right),$$

$$S_d = C_1^d \sin\left(\frac{8\pi L}{\lambda_m} + \eta_d\right)$$

has to be completed within $2L \leqslant 1.5D_{p,m}$ for Q_{avg} to exhibit nonmonotonicity. Since, number of wave cycles that can be formed within $2L = 1.5D_{p,m}$ is $1.5/n\pi$ if $S_{n,2}$ or S_d is the dominating mode and $1.5/2n\pi$ if $S_{n,1}$ is the dominating mode, hence, the bound on n for which Q_{avg} exhibits nonmonotonicity or resonance is obtained as

$$n \leqslant \begin{cases} \dfrac{1.5}{\pi} \text{ if } S_{n,2} \text{ or } S_d \text{ is the dominating mode} \\ \dfrac{1.5}{2\pi} \text{ if } S_{n,1} \text{ is the dominating mode} \end{cases} \tag{23}$$

where the amplitude of nonmonotonicity diminishes as n approaches $1.5/\pi$ or $1.5/2\pi$.

Within the range of Eq. 23, average absorbed power exhibits peaks around the minima of S_d if contribution of S_d is not negligible compared to C_0^d, which is the case for all p and n, except $p \approx 1$, where $C_1^d \ll C_0^d \; \forall L$ (refer to Eqs. B3d and 3e). In such cases of $p \approx 1$, average absorbed power exhibits nonmonotonicity due to either $S_{n,1}$ or $S_{n,2}$ if $C_0^n \not\gg \min\{C_1^n, C_2^n\}$ for $2L \leqslant 1.5D_{p,m}$. However, it follows from Eqs. B3a and 3c that $C_0^n \gg C_2^n \; \forall \; \{p \approx 1, n \leqslant 1.5/2\pi, \phi_l, \phi_r\}$, which results $S_{n,1}$ to be the only responsible mode for nonmonotonicity in average absorbed power for $p \approx 1$. Consequently, $Q_{avg}|_{p\approx 1}$ does not show any nonmonotonicity for one-side incidence (ϕ_l or $\phi_r \approx 0$), where $S_{n,1}$ drops out of Eq. 21. This is illustrated in Figure 2, which plots Q_{avg} vs. $2L/\lambda_m$ for $p = 1$, $n = 0.001$, 0.01, 0.1, and 0.2 in subplots (a), (b), (c), and (d), respectively, and $\phi_l = 0$ (continuous lines), 1/8 (dashed lines), 1/4 (dashed-dotted lines), 1/3 (dots), and 1/2 (bullets). As $Q_{avg}|_{\phi_l=j} = Q_{avg}|_{\phi_l=1-j}$, $0 \leqslant j \leqslant 1$ for $\kappa_l = \kappa_r$, Q_{avg} for $1/2 \leqslant \phi_l \leqslant 1$ exactly correspond to those for $1/2 \geqslant \phi_l \geqslant 0$, and will not be shown here. It can be seen from Figure 2 that nonmonotonicity in $Q_{avg} \; \forall \; \{n, p \approx 1\}$ appears for ϕ_l or $\phi_r \neq 0$, where the location of resonating peaks (denoted by L_{R_j}, $j = 1, 2 \ldots$) correspond to the maxima of $S_{n,1}$, and can be

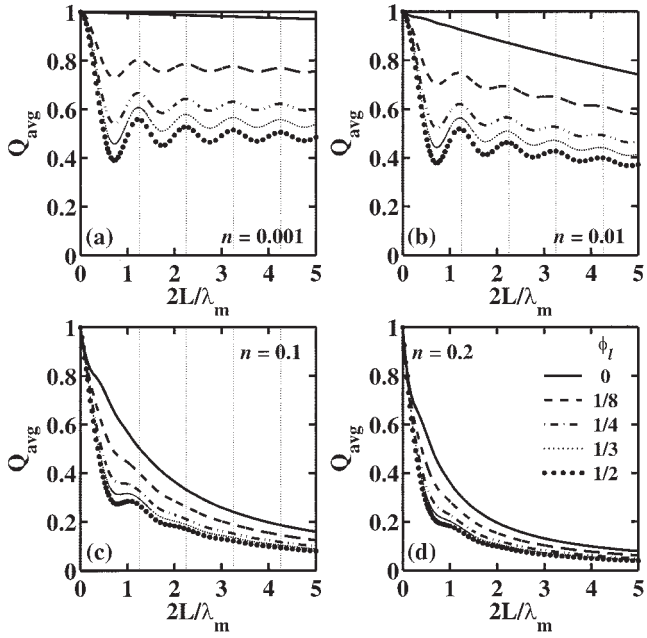

Figure 2. Resonating characteristics of Q_{avg} vs. $2L/\lambda_m$ for $p = 1$, $n = 0.001$, 0.01, 0.1, and 0.2 in subplots (a), (b), (c), and (d), respectively, and $\phi_l = 0$ (continuous lines), 1/8 (dashed lines), 1/4 (dash-dotted lines), 1/3 (dotted lines), and 1/2 (bullets).

predicted from the following relation obtained via asymptotic expansion

$$\frac{2L_{R_j}}{\lambda_m} = \frac{4j+1}{4} + \frac{\delta_{c,j}}{\pi}, \quad j = 1, 2, 3 \ldots \tag{24a}$$

where

$$\delta_{c,j} = \frac{-c_{j,2}^{\delta} - \sqrt{(c_{j,2}^{\delta})^2 - 4c_{j,3}^{\delta}c_{j,1}^{\delta}}}{2c_{j,3}^{\delta}} \tag{24b}$$

with the coefficients $c_{j,1}^{\delta}$, $c_{j,2}^{\delta}$, and $c_{j,3}^{\delta}$ given in Appendix C. It may be noted from Eq. B3f that $\eta_{n,1} \to 0$ in the limit of $p \to 1$, and $n \ll 1.5/2\pi$ (refer to Appendix B), which results in $\delta_{c,j} \to 0$ simplifying Eq. 24a to

$$\frac{2L_{R_j}}{\lambda_m} = \frac{4j+1}{4}, \quad j = 1, 2, 3 \ldots \tag{25}$$

Thus, peaks of $Q_{avg}|_{p\to 1, n\to 0}$ occur at $2L/\lambda_m = 1.25$, 2.25, 3.25, and so on, as can be seen from Figure 2a and b. Note that, L_{R_j}'s corresponding to Eq. 25 are shown in vertical dotted lines in Figure 2a–c. For other $n \leqslant 1.5/2\pi$ and $p \approx 1$, L_{R_j} deviates significantly from Eq. 25 (see Figure 2c), which can be predicted by Eq. 24a as reported in Table 1. In Table 1, $2L_{R_1}/\lambda_m$ for $\phi_l = 1/2$ and 1/4, and various n and p values within the range $0.001 \leqslant n \leqslant 0.1$ and $0.9 \leqslant p \leqslant 1.1$ have been listed corresponding to both Eqs. 21 and 24a, which shows good agreement between the two. It can be noted from Table 1 that

Table 1. $2L_{R_1}/\lambda_m$ Corresponding to Eqs. 21 and 24a for $\phi_l = 1/2$ and 1/4, $0.001 \leqslant n \leqslant 0.1$ and $p \approx 1$

	$p = 0.9$	$p = 0.95$	$p = 1$	$p = 1.05$	$p = 1.1$	
			$\phi_l = 1/2$			
$n = 0.001$	1.1223	1.1665	1.2279	1.2989	1.3584	Eq. 21
	1.1392	1.1752	1.2280	1.2903	1.3402	Eq. 24a
$n = 0.01$	1.1133	1.1548	1.2131	1.2829	1.3443	Eq. 21
	0.1303	1.1641	1.2139	1.2751	1.3269	Eq. 24a
$n = 0.05$	1.0701	1.0983	1.1397	1.1965	1.2600	Eq. 21
	1.0884	1.1135	1.1495	1.1983	1.2523	Eq. 24a
$n = 0.1$	1.0098	1.0209	1.0388	1.0684	1.1143	Eq. 21
	1.0310	1.0481	1.0709	1.1014	1.1404	Eq. 24a
			$\phi_l = 1/4$			
$n = 0.001$	1.1169	1.1621	1.2271	1.3032	1.3647	Eq. 21
	1.1387	1.1746	1.2272	1.2895	1.3395	Eq. 24a
$n = 0.01$	1.1043	1.1448	1.2042	1.2790	1.3451	Eq. 21
	1.1256	1.1579	1.2058	1.2661	1.3193	Eq. 24a
$n = 0.05$	1.0419	1.0595	1.0869	1.1314	1.2005	Eq. 21
	1.0643	1.0831	1.1105	1.1505	1.2022	Eq. 24a
$n = 0.1$	0.9447	0.9189	No peak	No Peak	No peak	Eq. 21
	0.9797	0.9868	—	—	—	Eq. 24a

for each n, L_{R_1}/λ_m decreases for $p \lessapprox 1$, while increases for $p \gtrapprox 1$ compared to $p = 1$. It can also be noted that $2L_{R_1}/\lambda_m \rightarrow 1$ as n approaches $1.5/2\pi$, where $\delta_{c,1} \rightarrow -\pi/4$. However, due to dominance of C_0^n over C_1^n near $n \leqslant 1.5/2\pi$, the region of nonmonotonicity is restricted to $n \ll 1.5/2\pi$ resulting in a monotonic decay of Q_{avg} ($n = 0.2$, $p = 1$) $\forall \phi_l$ in Figure 2d.

For all other p, such that $p \not\approx 1$, the resonating peaks of Q_{avg} occur around the minima of S_d, where jth resonating length (L_{R_j}) can be predicted from the following relation, which is obtained via an asymptotic expansion

$$\frac{2L_{R_j}}{\lambda_m} = \frac{(4j-1)}{8} - \frac{\eta_d}{4\pi} + \frac{\delta_{c,j}}{\pi}, \quad j = 1, 2, 3, \ldots \tag{26}$$

where $\delta_{c,j}$ is given by

$$\delta_{c,j} = -\left.\frac{n(c_{q,4}^d \cosh n\varepsilon_c + c_{q,2}^d \sinh n\varepsilon_c)}{4(C_1^d + n^2(c_{q,2}^d \cosh n\varepsilon_c + c_{q,4}^d \sinh n\varepsilon_c))}\right|_{\varepsilon_c=(4j-1)(\pi/2)-\eta_d} \quad \forall \{p \gg 1, n \approx 1.5/\pi\} \tag{27a}$$

and

$$\delta_{c,j} = -\left.\frac{n(c_{q,4}^4 \cosh n\varepsilon_c + c_{q,2}^4 \sinh n\varepsilon_c)}{4(1+n^2)(c_{q,2}^4 \cosh n\varepsilon_c + c_{q,4}^4 \sinh n\varepsilon_c)}\right|_{\varepsilon_c=(4j-1)(\pi/2)-\eta_d} \tag{27b}$$

otherwise. The predictions of above relations are compared with exact location of $2L_{R_1}/\lambda_m$ corresponding to Eq. 21 in Table 2 for $\phi_l = 0$, $p = 0.01$, 0.1, 1, 10, and $0.001 \leqslant n \leqslant 0.4$. It may be noted that $2L_{R_1}/\lambda_m \rightarrow 0.5$ as $n \rightarrow 0$, which follows from the fact that $n_d|_{n \ll 1} \approx -\pi/2$ (refer to Eq. B3h) simplifying Eq. 26 to

$$\left.\frac{2L_{R_j}}{\lambda_m}\right|_{n \ll 1} = \frac{j}{2} + \frac{\delta_{c,j}}{\pi}, \quad j = 1, 2, 3 \ldots \tag{28}$$

where $\delta_{c,j}|_{n \rightarrow 0} \rightarrow 0$. [Remark: Eq. 28 without the correction term ($\delta_{c,j}$) was obtained by earlier researchers (Ayappa et al., 1997; Ayappa, 1999) with a least square fit of numerically obtained data points for some specific materials for example, water, oil, and so on, which satisfy the condition $n \ll 1$]. As n approaches $1.5/\pi$, $2L_{R_1}/\lambda_m$ deviates significantly from 0.5, which can be efficiently predicted by Eq. 26 as can be seen from Table 2. The deviations of $2L_{R_1}$ from $0.5\lambda_m$ as n varies from 0 to $1.5/\pi$ are also shown in Figure 3 for $\phi_l = 0$ (in subplots (a) and (c)) and 1/4 (in subplots (b) and (d)), $p = 0.1$ (in subplots (a)–(b)), and 10 (in subplots (c)–(d)), and $n = 0.1$ (continuous lines), 0.2 (dashed lines), 0.3 (dash-dotted lines), 0.4 (dotted lines). In Figure 3, the exact locations of $2L_{R_1}/\lambda_m$ are indicated by markers, while vertical dotted lines are drawn at $2L/\lambda_m = 0.5$. This figure clearly shows that the resonating peaks of Q_{avg} for $n \ll 1$ can be predicted by Eq. 28 with $\delta_{c,j} = 0$, while $2L_{R_j}/\lambda_m$ differs significantly from $j/2$ as n approaches $1.5/\pi$. Note that this exact analysis was completely overlooked by earlier researchers. It may also be noted that the amplitude of nonmonotonicity diminishes with increasing n finally vanishing in the limit of $n \rightarrow 1.5/\pi$ due to increasing dominance of C_0^d over C_1^d with increasing n.

It is important to mention that doubling the frequency from $S_{n,1}$ to S_d along with the phase difference between the two given in Appendix B (Eqs. B3f and 3h), cause every alternate minima of S_d to be located near a minima of $S_{n,1}$ $\forall p$ and n satisfying Eq. 23. This might result in suppression of the peaks of Q_{avg} at the corresponding resonating points, where a minima of S_d is located near a minima of $S_{n,1}$ giving rise to nonmonotonic decay of subsequent resonating peaks of Q_{avg}. It may also be mentioned that the suppression of peaks occurs due to the interaction of multimode sine waves ($S_{n,1}$ and S_d). Thus, the suppression is absent for either one side incidence, where S_d governs the nonmonotonicity of Q_{avg} or both-side incidence

Table 2. $2L_{R_1}/\lambda_m$ Corresponding to Eqs. 21 and 26 with $\delta_{c,1}$ Given by Eq. 27a, b for $\phi_l = 0$, $0.001 \leq n \leq 0.4$ and $p \neq 1$

	$p = 0.01$	$p = 0.1$	$p = 10$	$p = 100$	
$n = 0.001$	0.5	0.5010	0.4990	0.5	Eq. 21
	0.5	0.4999	0.5	0.5	Eq. 26 with Eq. 27b
	0.5	0.4999	0.5	0.5	Eq. 26 with Eq. 27a
$n = 0.01$	0.5	0.5007	0.4986	0.4999	Eq. 21
	0.4999	0.4993	0.5	0.5	Eq. 26 with Eq. 27b
	0.4999	0.4993	0.4999	0.5	Eq. 26 with Eq. 27a
$n = 0.05$	0.4992	0.4987	0.4955	0.4980	Eq. 21
	0.4985	0.4960	0.4992	0.4988	Eq. 26 with Eq. 27b
	0.4984	0.4953	0.4985	0.4987	Eq. 26 with Eq. 27a
$n = 0.1$	0.4971	0.4949	0.4884	0.4923	Eq. 21
	0.4951	0.4907	0.4971	0.4957	Eq. 26 with Eq. 27b
	0.4940	0.4873	0.4936	0.4947	Eq. 26 with Eq. 27a
$n = 0.2$	0.4887	0.4825	0.4639	0.4711	Eq. 21
	0.4862	0.4797	0.4922	0.4875	Eq. 26 with Eq. 27b
	0.4745	0.4586	0.4696	0.4756	Eq. 26 with Eq. 27a
$n = 0.3$	0.4732	0.4620	0.4267	0.4389	Eq. 21
	0.4781	0.4698	0.4882	0.4800	Eq. 26 with Eq. 27b
	0.4386	0.4147	0.4273	0.4399	Eq. 26 with Eq. 27a
$n = 0.4$	0.4483	0.4305	0.3774	0.3978	Eq. 21
	0.4718	0.4617	0.4856	0.4742	Eq. 26 with Eq. 27b
	0.3995	0.3764	0.3917	0.4010	Eq. 26 with Eq. 27a

with equal power input from left and right sides ($\phi_l = \phi_r = 1/2$), where Eq. 21 can be simplified to

$$Q_{avg} = \frac{p^2\left(n \sin\frac{4\pi L}{\lambda_m} + \sinh\frac{2L}{D_{p,m}}\right)}{2\varepsilon_l \sinh\frac{2L}{D_{p,m}} + (1 + n^2 + p^2)\cosh\frac{2L}{D_{p,m}} - (1 + n^2 - p^2)\cos\frac{4\pi L}{\lambda_m} + 2np \sin\frac{4\pi L}{\lambda_m}} \quad (29)$$

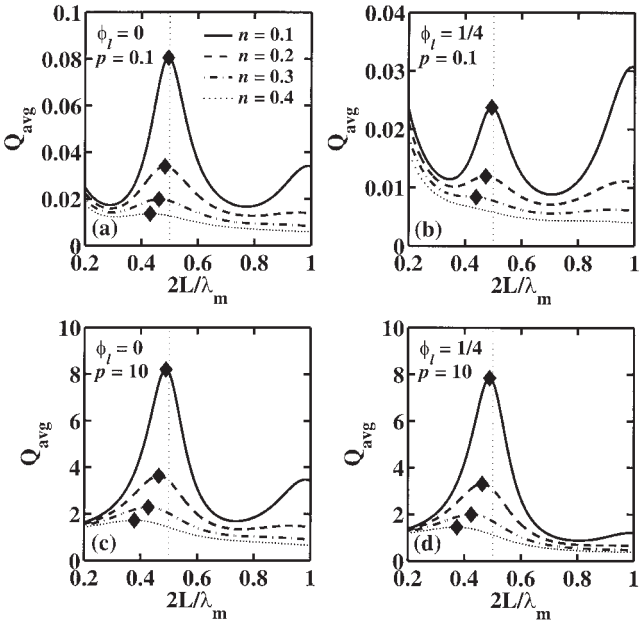

Figure 3. Location of first resonating peak of Q_{avg} for $\phi_l = 0$ (in subplots (a) and (c)) and 1/4 (in subplots (b) and (d)), $p = 0.1$ in subplots (a)–(b) and 10 in subplots (b)–(d) and $n = 0.1$ (continuous lines), 0.2 (dashed lines), 0.3 (dash-dotted lines), 0.4 (dotted lines).

It immediately follows that, a single mode sine wave of frequency $2/\lambda_m$ determines the nonmonotonic features of Q_{avg} for $\phi_l \approx \phi_r$. Suppression of resonating peaks is also absent for $p \approx 1$, where $S_{n,1}$ dictates the resonating features of Q_{avg} leading to monotonic decay of resonating peaks as can be seen from Figure 2. It may be noted from Eqs. B3f and 3h that both η_d and $\eta_{n,1}$ are negative for $p \gg 1$, while η_d is negative but $\eta_{n,1}$ is positive for $p \ll 1$. As a result, the suppression of peaks for ϕ_l or $\phi_r \neq 0$, 1, or 1/2, occurs at odd resonating points ($j = 1, 3, 5 \ldots$ in Eq. 26) for $p \ll 1$ or at even resonating points ($j = 2, 4, 6 \ldots$ in Eq. 26) for $p \gg 1$ as shown in Figure 4, which plots Q_{avg} vs. $2L/\lambda_m$ for $n = 0.01$, $p = 0.1$ (in subplot (a)), and 10 (in subplot (b)), and $\phi_l = 0$ (continuous lines), 1/8 (dashed lines), 1/4 (dash-dotted lines), 1/3 (dotted lines), and 1/2 (bullets). As explained earlier, nonmonotonic decay of resonating peaks occur for $\phi_l \neq 0$ and 1/2 (see inset plots) due to the suppression of odd (in subplot (a)) or even (in subplot (b)) resonating peaks, where the suppression increases as ϕ_l or ϕ_r varies from 0 to 1/2 (or 1 to 1/2) finally eliminating the corresponding peaks for $\phi_l \approx \phi_r = 1/2$ (see the inset plots). Thus, Q_{avg} with ϕ_l or $\phi_r \approx 1/2$ exhibits peaks around $2L_{R_j}/\lambda_m \approx j$ for $p < 1$, and $2L_{R_j}/\lambda_m = j - 1/2$ for $p > 1$, $j = 1, 2, 3 \ldots$, where the locations of resonating peaks can be predicted from either Eq. 24a for $p \approx 1$ (refer to Table 1), or Eq. 26 corresponding to $j = 2, 4, 6 \ldots$ for $p < 1$ and $j = 1, 3, 5 \ldots$ for $p > 1$ as shown in Table 3. Table 3 lists $2L_{R_1}/\lambda_m$ corresponding to Eqs. 21 and 26 for $\phi_l = 1/2$, $p = 0.01$, 0.1, 10, and 100, and $0.001 \leq n \leq 0.4$. It may be noted that the exact location of $2L_{R_1}/\lambda_m$ can be efficiently predicted by Eq. 26, where Eq. 27b predicts much better than Eq. 27a for $p \gg 1$ and $n \not\ll 1.5/\pi$ or vice versa.

The suppression of peaks also increases with either decreasing n (where C_1^n dominates over C_1^d) or increasing sample length due to exponential increase of C_0^n and C_0^d as shown in Figure 5, which plots Q_{avg} vs. $2L/D_{p,m}$ for $\phi_l = 1/4$, $n = 0.001$ (in subplots (a), (d), (g)), 0.01 (in subplots (b), (e), (h)), and 0.1 (in subplots (c), (f), (i)). Here, the results are plotted for $p = 0.1$ in subplots (a)–(c), 1 in subplots (d)–(f), and 10 in subplots (g)–(i). This figure also shows that nonmonotonicity

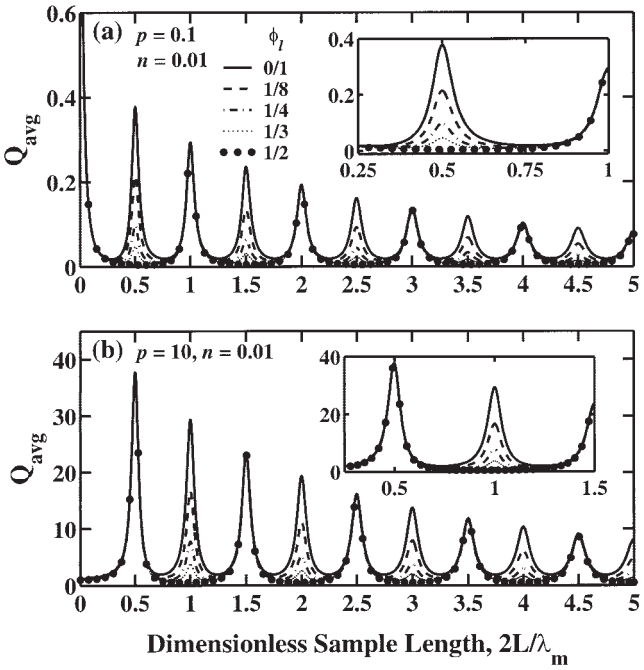

Figure 4. Dimensionless average power (Q_{avg}) vs. $2L/\lambda_m$ for $n = 0.01$, $p = 0.1$, and 10 in subplots (a) and (b), respectively, and $\phi_l = 0$ (continuous lines), 1/8 (dashed lines), 1/4 (dash-dotted lines), 1/3 (dotted lines), and 1/2 (bullets).

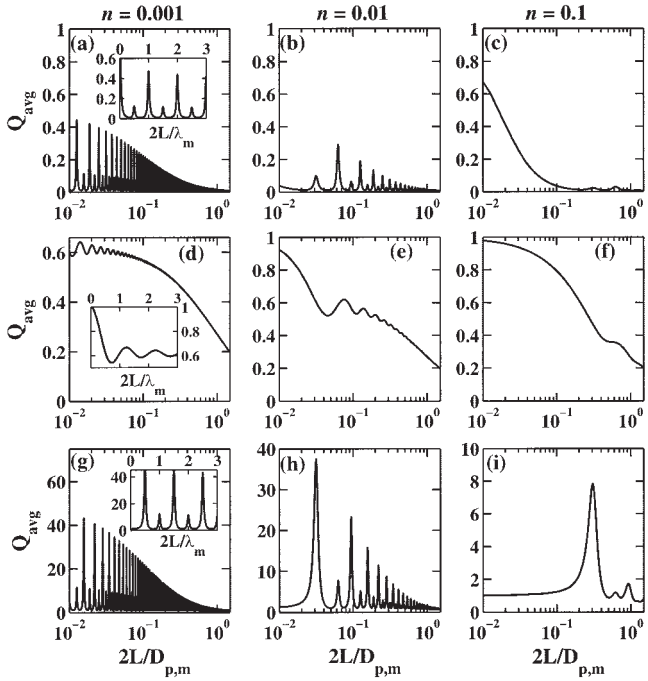

Figure 5. Monotonic and nonmonotonic decay of resonating peaks of Q_{avg} vs. $2L/D_{p,m}$ plots for $\phi_l = 1/4$, $n = 0.001$ (subplots (a), (d), (g)), 0.01 (subplots (b), (e), (h)), and 0.1 (subplots (c), (f), (i)), and $p = 0.1$ (subplots (a)–(c)), 1 (subplots (d)–(f)), and 10 (subplots (g)–(i)).

of Q_{avg}, which decreases with increasing n, vanishes for $2L/D_{p,m} \gg 1$, while subsequent resonating peaks decay either monotonically (for $p \approx 1$) or nonmonotonically (for $p \not\approx 1$). It may be noted that nonmonotonicity of Q_{avg} for $p \approx 1$ is much less prominent than $p \not\approx 1$ for all parameter values, which is due to the fact that C_0^n dominates over C_1^n much stronger than C_0^d does over C_1^d (refer to Eqs. B3a–3e). As a result, nonmonotonicity of Q_{avg} vanishes at much smaller sample length for $p \approx 1$ than $p \not\approx 1$ as can be seen from Figure 5. It can also be noted that the suppression of peaks increases with either decreasing n or increasing sample length for the reasons mentioned earlier.

Outside the range of Eq. 23, average absorbed power may exhibit a single peak within $2L \leqslant 1.5D_{p,m}$ if Q_{avg} has increasing dependency on sample length within the thin sample regime, where Q_{avg} can be written as

Table 3. $2L_{R_1}/\lambda_m$ Corresponding to Eqs. 21 and 26 with $\delta_{c,1}$ Given by Eq. 27a, b for $\phi_l = 1/2$, $0.001 \leqslant n \leqslant 0.4$, and $p \not\approx 1$

	$p = 0.01$	$p = 0.1$	$p = 10$	$p = 100$	
$n = 0.001$	1	1.0005	0.4989	0.5	Eq. 21
	1	0.9999	0.5	0.5	Eq. 26 with Eq. 27b
	1	0.9999	0.5	0.5	Eq. 26 with Eq. 27a
$n = 0.01$	0.9999	1.0001	0.4986	0.4999	Eq. 21
	0.9998	0.9993	0.5	0.5	Eq. 26 with Eq. 27b
	0.9998	0.9992	0.4999	0.5	Eq. 26 with Eq. 27a
$n = 0.05$	0.9986	0.9976	0.4954	0.4980	Eq. 21
	0.9975	0.9953	0.4992	0.4988	Eq. 26 with Eq. 27b
	0.9970	0.9936	0.4985	0.4987	Eq. 26 with Eq. 27a
$n = 0.1$	0.9946	0.9921	0.4880	0.4922	Eq. 21
	0.9929	0.9895	0.4971	0.4957	Eq. 26 with Eq. 27b
	0.9865	0.9774	0.4936	0.4947	Eq. 26 with Eq. 27a
$n = 0.2$	0.9781	0.9718	0.4622	0.4704	Eq. 21
	0.9843	0.9786	0.4922	0.4875	Eq. 26 with Eq. 27b
	0.9188	0.8895	0.4696	0.4756	Eq. 26 with Eq. 27a
$n = 0.3$	0.9476	0.9366	0.4228	0.4367	Eq. 21
	0.9772	0.9693	0.4882	0.4800	Eq. 26 with Eq. 27b
	0.8219	0.7972	0.4273	0.4399	Eq. 26 with Eq. 27a
$n = 0.4$	0.8984	0.8804	0.3717	0.3938	Eq. 21
	0.9715	0.9615	0.4856	0.4742	Eq. 26 with Eq. 27b
	0.8147	0.8015	0.3917	0.4010	Eq. 26 with Eq. 27a

Table 4. First Feasible Root of Eq. 31 (ε_{R_1}) for $n \geq 1.5/\pi$, $p > 1$, and $\phi_l = 0$ and 1/2

	$p = 2.5$	$p = 5$	$p = 10$	$p = 100$	$p = 5$	$p = 10$	$p = 100$
		$\phi_l = 0$				$\phi_l = 1/2$	
$n = \frac{1.5}{\pi}$	0.1777	0.022	0.0028	2.8×10^{-6}	—	0.196	0.0186
$n = 0.5$	0.1052	0.023	0.003	3×10^{-6}	—	0.213	0.020
$n = 0.6$	—	0.028	0.0036	3.6×10^{-6}	—	0.3333	0.0282
$n = 0.7$	—	0.0332	0.0042	4.2×10^{-6}	—	—	0.0413
$n = 0.8$	—	0.0387	0.0048	4.8×10^{-6}	—	—	0.0676
$n = 0.9$	—	0.0448	0.0054	5.4×10^{-6}	—	—	0.1888
$n = 1$	—	0.0515	0.006	6×10^{-6}	—	—	—

$$Q_{avg} = \frac{1 + a_1\varepsilon_R^2 + a_2\varepsilon_R^3 + a_3\varepsilon_R^4}{1 + b_1\varepsilon_R + b_2\varepsilon_R^2 + b_3\varepsilon_R^3 + b_4\varepsilon_R^4}, \quad 2L < L_{min} \tag{30}$$

with ε_R defined in Eq. 18, and coefficients a_i and b_i given in Appendix D. It follows from Eq. 30 that there always exists a set of L near $\varepsilon_R \to 0$ for which Q_{avg} decreases with increasing sample length as $O(\varepsilon_R)$ term, which is positive in the denominator, is missing from the numerator. This along with the fact that maximum number of full wave cycles that can be formed within L_{min} is $1/\pi$ infers that if Eq. 23 is satisfied, then the first peak of Q_{avg} occurs outside thin-sample regime. Otherwise, Q_{avg} either follows a monotonic decay for $\forall L$ or exhibits a single peak within $2L \leq 1.5D_{p,m}$ depending on whether Eq. 30 is a monotonic or nonmonotonic function of L, respectively. Therefore, the condition for Q_{avg} vs. L plots to have a single maxima when Eq. 23 is not satisfied is obtained as the existence of at least one root of the following equation

$$\frac{dQ_{avg}}{d\varepsilon_R} = 0 \tag{31}$$

within $0 < \varepsilon_R \leq (1/2)\min\{1, (1/n)\}$ or $0 < \varepsilon_R \leq (1/2)$ since $n \leq 1$ according to Eq. 5a and b.

It follows from the fact that minimum sample length required to form a full wave is $\varepsilon_R = \pi/2$, Eq. 31 can have at the most two feasible roots denoted by ε_{R_1} and ε_{R_2} with $\varepsilon_{R_1} < \varepsilon_{R_2}$, where first root ε_{R_1} appears for $2L \ll L_{min}$, where Eq. 31 can be written as

$$\sum_{j=0}^{6} \tau_j \varepsilon_R^j = 0, \tag{32}$$

with the coefficients τ_j's given in Appendix D. Thus, in order for Eq. 31 to possess at least one feasible root, τ_1 should be positive (as τ_0 is negative $\forall\{n, p\}$, see Eq. D2a) along with the condition $|\tau_1| \gg 2|\tau_0|$. This leads to the conclusion that p has to be $\gg 1$ (with exact value depending on n and ϕ_l) in order to have a single peak in Q_{avg} outside the boundary of Eq. 23, where the peak appears either at ε_{R_2} whenever exists or within $2L \leq 1.5D_{p,m}$. It can be seen from Eq. D2b that the p value at which Q_{avg} starts exhibiting a single peak outside the range of Eq. 23 increases with increasing n. It also increases as ϕ_l varies from 0 to 1 to 1/2 vanishing all the feasible roots of Eq. 31 at $\phi_l = 1/2$ and $n \geq 1$, where Q_{avg} does not show any peak. However, $Q_{avg}|_{\phi_l = 1/2}$ may have a single peak for $1.5/\pi < n < 1$ if the conditions specified earlier are satisfied. This can be seen from Table 4, which lists ε_{R_1} for $1.5/\pi \leq n \leq 1$, $2.5 \leq p \leq 100$, and $\phi_l = 0$ and 1/2. It may be noted from Eq. D2a and 2b that the first root of Eq. 31 (denoted by ε_R) moves towards smaller ε_R as p increases or n decreases, which is also apparent from Table 4.

The earlier features are illustrated in Figure 6, which plots Q_{avg} vs. $2L/D_{p,m}$ for $p = 0.1$ (in subplots (a), (d), (g)), 10 (in subplots (b), (e), (h)), and 100 (in subplots (c), (f), (i)) and $n = 0.8$ (in subplots (a)–(c)), 0.9 (in subplots (d)–(f)), and 1 (in subplots (g)–(i)). Here, results are shown for $\phi_l = 0$ (continuous lines), 1/8 (dashed lines), 1/4 (dash-dotted lines), 1/3 (dotted lines), and 1/2 (bullets), while the insets show Q_{avg} vs. $2L/\lambda_m$ for $\phi_l = 0$. As can be seen from Figure 6, for fixed p, the location of single peak moves towards higher-sample

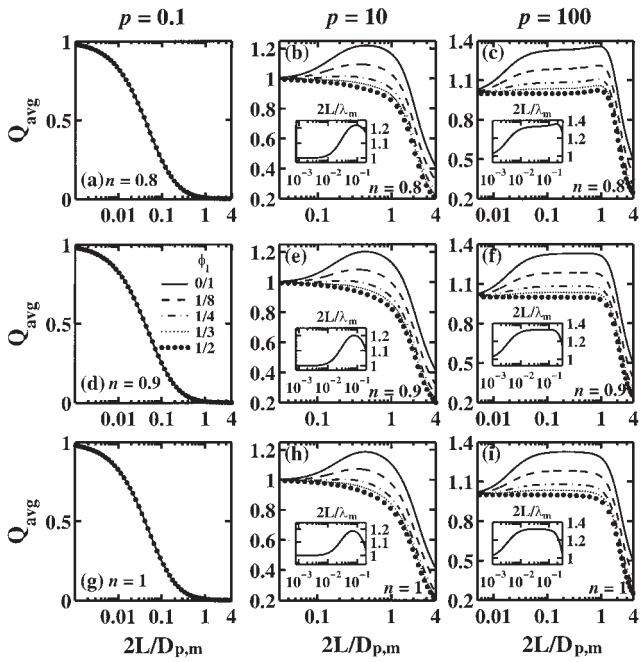

Figure 6. Presence of single peak in Q_{avg} vs. $2L/D_{p,m}$ plots outside the range of Eq. 23 for $n = 0.8$ (subplots (a)–(c)), 0.9 (subplots (d)–(f)), and 1 (subplots (g)–(i)), $p = 0.1$ (subplots (a), (d), (g)), 10 (subplots (b), (e), (h)), and 100 (subplots (c), (f), (i)) and $\phi_l = 0$ (continuous lines), 1/8 (dashed lines), 1/4 (dash-dotted lines), 1/3 (dotted lines), and 1/2 (bullets).

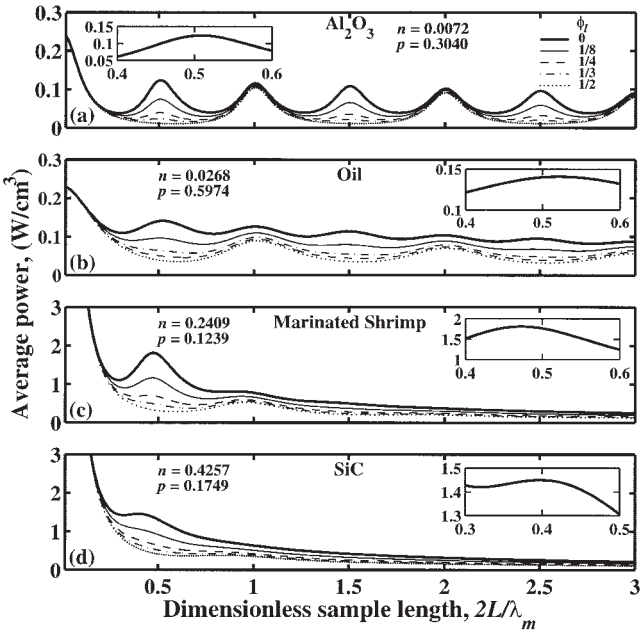

Figure 7. Average power (W cm^{-3}) vs. $2L/\lambda_m$ plots of Alumina, oil, marinated shrimp, and SiC for $\phi_l = 0$ (thick continuous lines), 1/8 (thin continuous lines), 1/4 (dashed lines), 1/3 (dash-dotted lines), and 1/2 (dotted lines).

length as n decreases from 1. This eliminates the 2nd feasible root of Eq. 31, as n approaches Eq. 23 for constant p (as in the case of $p = 100$ in Figure 6, see subplots (c), (f), and (i)), where the peak of Q_{avg} for n outside the range of Eq. 23, and p satisfying the conditions mentioned earlier occur within $n < 2L/D_{p,m} < 1.5$.

Efficient material processing: heating dynamics vs. average power characteristics

Figure 7 illustrates the average power characteristics for various food (oil and marinated shrimp) and ceramic (Alumina and SiC) materials. The dielectric and thermal properties of different materials are listed in Table 5, along with their n and p values. It is observed that among the food and ceramic materials chosen, n is smallest for Alumina, and is in ascending order with oil, shrimp, and SiC. Therefore, based on the theoretical analysis given in the previous section, the average power exhibits resonances at $2L_{R_j} = j/2$ for Alumina, as can be seen from Figure 7. The deviations of the location of resonating peaks from $2L_{R_j} = j/2$ increase from oil to shrimp and to SiC (see in the inset plots, which show the location of first resonating peak of average power for one side incidence, that is, $\phi_l = 0$) due to increasing n values, which can be predicted by Eq. 26. It may be interesting to note that, average absorbed power for materials with higher n values reach the exponential phase or thick sample regime at much smaller $2L/\lambda_m$. This is due to the fact that contribution from exponential position dependency of Q_{avg} increases with n, as discussed in the previous section. This is also reflected as a reduction of number of resonating peaks in Q_{avg} for Alumina, oil, shrimp, and SiC (see Figure 7). It may be noted that the decay of the average power at subsequent resonating peaks is much more pronounced for materials with higher n. Moreover, since $n = 0.4257$ tends to the outer range of Eq. 23 given by 0.477, the resonating features of average power are almost absent in SiC, as can be predicted from the theoretical analysis presented in the previous section. Therefore, n plays a critical role in deciding whether the absorbed power can be enhanced by selecting the sample thicknesses corresponding to various resonating modes. Furthermore, it may be observed that $p < 1$ for all the materials leading to suppression of odd (first, third, and so on) peaks as ϕ_l varies from 0 to 1/2. Thus, the absorbed power within a sample of thickness corresponding to the odd resonating modes can be tuned by selecting proper distribution of microwave source. It may be mentioned that the maxima in absorbed power may result in spatial hot spot within a sample, and a proper distribution of microwave incidence, thus, may be suitable for reducing hot spots as discussed later.

The hot spot formation during material processing can be deduced from temperature dynamics, which can be obtained by solving the following energy balance equation with associated initial and boundary conditions

$$\rho C_p \frac{\partial T}{\partial t} = k \frac{\partial^2 T}{\partial z'^2} + q(z'), \quad -L \leq z' \leq L \tag{33a}$$

$$\mp k \frac{\partial T}{\partial z'} = h(T - T_\infty) \quad @\ z' = \pm L \tag{33b}$$

$$T = T_0 \quad @\ t = 0 \tag{33c}$$

Here ρ is the density, C_p is the specific heat, k is the thermal conductivity, $q(z')$ is the volumetric heat generation due to microwave power absorption as given in Eq. 15, T_∞ is the

Table 5. Thermal and Dielectric Properties of Various Food and Ceramic Materials (Ayappa et al., 1991; Oliveira and Franca, 2002; Basak and Priya, 2005)

Material	λ_m (cm)	$D_{p,m}$ (cm)	$n = \frac{\lambda_m}{2\pi D_{p,m}}$	$p = \frac{\lambda_m}{\lambda_0}$	C_p ($kJ/kg°C$)	ρ (kg/m^3)	k (W/m°C)
Water	1.38	3.3	0.0665	0.1129	4.19	1000	0.609
Oil	7.31	43.47	0.0268	0.5974	2.0	900	0.168
Beef	1.84	1.73	0.1694	0.1503	2.51	1070	0.491
Marinated shrimp	1.52	1.0	0.2409	0.1239	2.5	1069	0.47
Non-marinated shrimp	1.56	1.41	0.1757	0.1275	2.5	1069	0.47
Al_2O_3	3.72	81.74	0.0072	0.3040	3.75	1046	26
SiC	2.14	0.8	0.4257	0.1749	3.3	3100	40

The dielectric properties correspond to 2450 MHz.

ambient temperature, T_0 is the initial temperature, and h is the heat-transfer coefficient. The convective term in Eq. 33a is neglected for liquid substances as the buoyancy driven convection in vertical direction is absent in semi-infinite slabs. Similar assumptions are also used in earlier works (Basak, 2003; Basak, 2004). Equation 33 has been solved using the similar manner, as discussed in earlier investigations (Basak, 2003; Basak, 2004) with $T_0 = T_\infty = 300$ K, and $h = 2$ W m^{-2} K^{-1}, and the results are shown in Figure 8 for oil and shrimp, and in Figure 9 for Alumina and SiC. Figures 8 and 9 illustrate the influence of various distribution of microwave incidence on temperature dynamics with identical total electric field $E_L + E_R = \sqrt{2I_0/c\varepsilon}$ ($I_0 = 3$ W cm^{-2}). The heating characteristics along with associated power distributions are shown for thin ($2L = 0.1\lambda_m$), resonating ($2L = 0.5\lambda_m$ and $2L = \lambda_m$), and thick ($2L = 3D_{p,m}$) sample regimes in order to establish the fact that temperature dynamics is a direct consequence of the generalized average power characteristics.

The average absorbed power for constant $E_L + E_R$ is found to be independent of distribution of microwave incidence in thin sample regime ($2L < \lambda_m/2\pi$) (see Figure 7) and as a consequence the heating characteristics are also invariant of ϕ_l as may be observed from Figures 8 and 9 for $2L = 0.1\lambda_m$. In this regime, almost uniform temperature distributions are attained within the sample, based on uniform thin sample asymptotes of absorbed power distributions as shown in Figures 8 and 9. Following the thin sample asymptote, uniform temperature distributions may be obtained up to the sample thickness corresponding to the upper bound of thin sample limit ($2L < \lambda_m/2\pi$). Therefore, materials with large wavelength (for example, Alumina and oil) can be processed uniformly up to a higher-sample thickness compared to the materials with smaller wavelength (for example, shrimp).

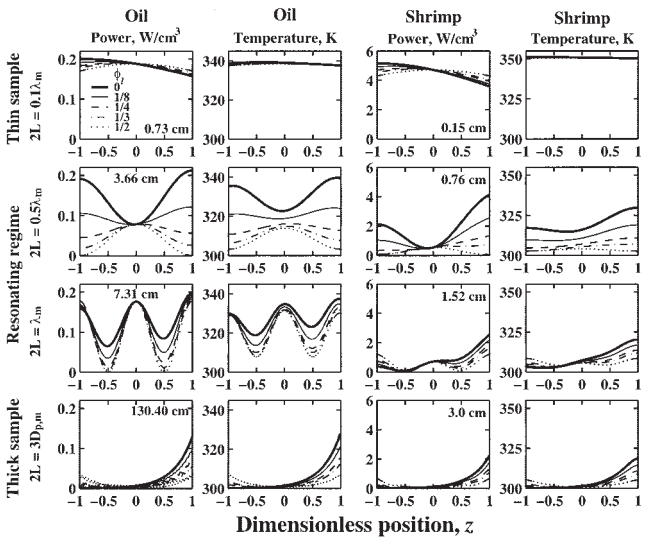

Figure 8. Absorbed power (W cm^{-3}) and temperature (K) distributions for food materials (oil and marinated shrimp) of thickness corresponding to thin ($2L = 0.1\lambda_m$), resonating ($2L = 0.5\lambda_m$ and $2L = 0.1\lambda_m$), and thick ($2L = 3D_{p,m}$) sample regimes.

The temperature profiles are shown at 100 s for oil and 45 s for shrimp.

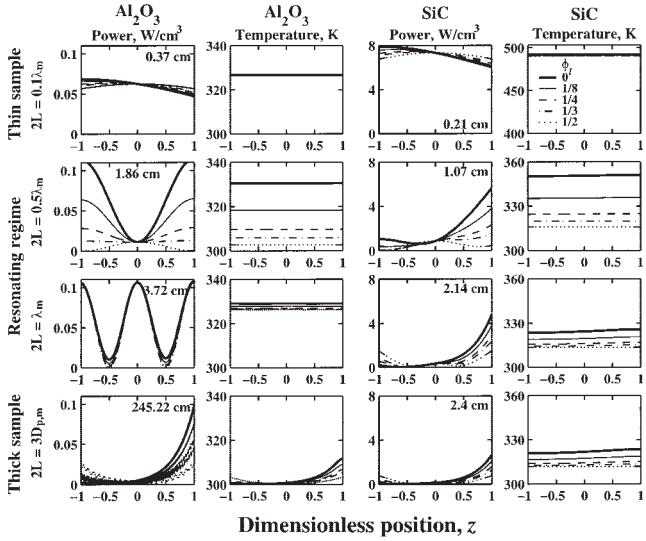

Figure 9. Absorbed power (W cm^{-3}) and temperature (K) distributions for ceramic materials (Alumina and SiC) of thickness corresponding to thin ($2L = 0.1\lambda_m$), resonating ($2L = 0.5\lambda_m$ and $2L = 0.1\lambda_m$), and thick ($2L = 3D_{p,m}$) sample regimes.

The temperature profiles are shown at 400 s for Alumina and 100 s for SiC.

On the other hand, absorbed power, as well as temperature distributions follow exponential decay within thick samples as shown in Figures 8 and 9 for $2L = 3D_{p,m}$. In this regime, temperature dynamics are dependent on the distribution of microwave incidence since the average absorbed power is a function of ϕ_l, as discussed in earlier sections. Therefore, the only hot spot occurring at the right surface for $\phi_l = 0$ can be significantly reduced by distributing the microwave incidence as shown in Figures 8 and 9 for varying ϕ_l to 1/8, 1/4, 1/3, and 1/2 (equal incidence from both side).

The resonating regime occurring within thin and thick sample limits are illustrated for $2L = 0.5\lambda_m$, and $2L = \lambda_m$. It is interesting to observe that as sample thickness increases, the number of spatial maxima in power distribution also increase. Therefore, the ratio $2L/\lambda_m$, which corresponds to number of maxima in average power also dictates the number of maxima in spatial-power distribution within the sample. This nonuniformity in absorbed-power distribution may initiate hot spots within the sample depending on the thermal properties of the material. For example, for the case of ceramic materials (Alumina and SiC) with high-thermal conductivity, the temperature distributions are always uniform within the sample irrespective of the spatial nonuniformity in absorbed power. On the other hand, for most of the food materials with low-thermal conductivity, the temperature distributions follow the power distributions. This results in higher probability of hot spot formation in the microwave processing of food materials, if the sample thickness is within resonating regime. Therefore, an important question that may arise is that whether it is possible to reduce the hot spot within resonating regime. This can be addressed from the average power vs. sample length plots (Figure 7). Since, the resonating peak in absorbed power at $2L = 0.5\lambda_m$ reduces and finally vanished as ϕ_l changes from 0 to 1/2, the

hot spot formation can also be significantly reduced by distributing the microwave source. On the other hand, at $2L = \lambda_m$ the hot spot formation can not be tuned by distributing the microwave source, since average power is weakly dependent on ϕ_l. It may be important to note that since ϕ_l has weaker role on the temperature dynamics at even resonating peaks, the identical heating rate can be achieved at $2L = \lambda_m$ by utilizing half the total incident flux for equal incidence from both sides ($\phi_l = 1/2$), compared to that for one-side incidence ($\phi_l = 0$). This is due to the fact that $I_L + I_R = 1.5$ W cm^{-2} for $\phi_l = 1/2$, and $I_L + I_R = 3$ W cm^{-2} for $\phi_l = 0$ with constant $E_L + E_R = \sqrt{2I_0/c\varepsilon_0}$, where $I_0 = 3$ W cm^{-2}.

Conclusions

We have presented a comprehensive theoretical analysis (for the first time) to characterize the resonating features of average absorbed power (Q_{avg}) in a 1-D slab exposed to microwave radiations from both sides. We have shown through a detailed analysis of the closed form solution for Q_{avg} derived from the first principle that microwave induced absorbed power can be exactly characterized by three-length scales, namely wavelength (λ_m) and penetration depth ($D_{p,m}$) within the sample, and wavelength within the free space (λ_0), and the intensities of incident radiations from left and right sides (ϕ_l, where ϕ_l is the fractional microwave energy input from left side). It has been shown that the resonating regime of Q_{avg} is restricted within two asymptotic limits of thin ($2L \ll \lambda_m/2\pi$) and thick ($2L \gg D_{p,m}$) sample regime, since absorbed power within the sample follows either uniform distribution (for thin sample) or exponential decay (for thick samples). Within the resonating regime, average absorbed power exhibits nonmonotonicity if $\lambda_m \leqslant 1.5D_{p,m}$ for $\lambda_m \approx \lambda_0$, and $\lambda_m \leqslant 3D_{p,m}$, otherwise. If the earlier conditions are satisfied, the occurrence of resonance is shown to be independent of the distribution of microwave source ($\forall \phi_l$) if $\lambda_m \not\approx \lambda_0$, while it is restricted to only both-side incidence ($\phi_l \not\approx 0$ or 1) for $\lambda_m \approx \lambda_0$. For $\lambda_m \approx \lambda_0$ and $\phi_l \not\approx 0$ or 1, the resonating peaks of Q_{avg} occur around $2L_{R_j}/\lambda_m \approx (4j + 1)/4$, where the exact locations depend on $\lambda_m/D_{p,m}$, λ_m/λ_0, and ϕ_l as can be predicted by Eq. 24a. On the other hand, Q_{avg} exhibits peaks at $2L_{R_j}/\lambda_m = (4j - 1)/8 - \eta_d/4\pi + \delta_{c,j}/\pi$ (refer to Eq. 26) for $\lambda_m \not\approx \lambda_0$ and $\phi_l \not\approx 1/2$, which reduces to $2L_{R_j}/\lambda_m = j/2 + \delta_{c,j}/\pi$ for $\lambda_m \ll 2\pi D_{p,m}$. In this case, even (for $\lambda_m > \lambda_0$) or odd (for $\lambda_m < \lambda_0$) resonating peaks get suppressed as ϕ_l varies from 0 or 1 (one side incidence) to 1/2 finally eliminating the corresponding peaks for equal power input from both sides ($\phi_l \approx 1/2$).

The closed form analysis presented here can be used as a guideline to obtain the quantitative measure of absorbed power during material processing. The average power distributions vs. $2L/\lambda_m$ are illustrated for food (oil and marinated shrimp) and ceramic (Alumina and SiC) materials. It is observed that the number of resonating peaks, and the maxima in average power corresponding to all peaks differ for materials; however the entire power spectrum is guided by n. It is interesting to note that the higher number of resonating peaks occurs for Alumina with $n = 0.0072$, and the average power decays almost exponentially with $2L/\lambda_m$ for SiC with $n = 0.4257$. It may be noted that the reduction of average power at subsequent peaks increases with n. As a direct consequence, alumina shows almost no reduction in average power at first few resonating peaks, while the average power shows only one resonating peak (for one side incidence) for SiC. The intermediate materials (Oil and Marinated Shrimp) correspond to $n = 0.0268$ and 0.2409, respectively, and, thus, the variation of average power can be forecasted, based on our generalized theoretical analysis. The role of distributed sources of microwaves can also be shown, and it is observed for the selected materials that the average power at odd resonating peaks tends to die off as the distribution ϕ_l increases from 0 to 1/2. This situation may be very important for material processing, as the distributed microwave incidence may play a critical role to trigger the hot spots and uniform heating.

The predictions of average power have a direct consequence on heating qualities for material processing as the overall heating rate ($d\bar{T}/dt$) is directly proportional to Q_{avg} as shown in the following equation

$$\rho C_p \frac{d\bar{T}}{dt} = Q_{avg} - \text{heat loss to the surrounding} \qquad (34)$$

The earlier equation has been obtained by integrating Eq. 33a-b, where $\bar{T}$ is the average temperature within the sample. Thus, the overall heating rate can be predicted from the average power (Q_{avg}) vs. sample length plots (Figure 7), and finally, the local heating effects can be directly correlated with the average power characteristics. At this point, it may be concluded that Figure 7 acts as a master curve to guide the prediction of overall heating rate within a material.

The average power within thin sample limit illustrates that almost uniform spatial temperature occurs for food and ceramic materials, whereas the hot spots occur at the exposed faces due to the maxima in spatial power in thick sample limits. The heating operation within thick sample limits may not be advisable due to the occurrence of surface hot spots. The hot spot may be controlled with distributed incidence, but hot spot, however, small, will remain at the surface. The average power at a resonating peak is directly related with the number of spatial maxima of power for all the materials. It is observed that the number of spatial maxima in power increases with the ratio $2L/\lambda_m$. This may lead to hot spots for some materials depending on thermal properties. In general, the ceramic materials do possess high-thermal conductivity, and, therefore, the uniform temperature profiles are found for ceramics even within resonating regimes. In contrast, the occurrence of hot spots directly corresponds to the spatial power maxima for food materials as food materials have smaller thermal conductivities. Therefore, the processing of food materials pose real challenges on the efficient processing strategies and consequently the hot spots can be effectively tuned with the suitable distribution of microwave incidence.

Overall, our strong theoretical analysis reveals interesting features on average power characteristics, and that has direct relevance on efficient thermal processing for various food and ceramic materials. The entire analysis may unfold some of the optimal heating characteristics which may be guidelines for performing experimental studies with uniform plane waves.

Acknowledgment

Authors would like to thank the anonymous reviewer for constructive suggestions, which are valuable for improving the quality of the manuscript.

Notation

c = velocity of light, m s^{-1}
C_p = specific heat of the sample, J Kg^{-1} K^{-1}
$D_{p,m}$ = penetration depth within the sample, m
$D_{p,i}$ = penetration depth within ith medium, m
E_L (E_R) = incident electric field from left (right) side, V m^{-1}
E_T = total incident electric field, V m^{-1}
$E_{1,i}$ ($E_{2,i}$) = coefficient of transmission (reflection) in ith medium, V m^{-1}
$E_{x,m}$ = electric field within the sample, V m^{-1}
$E_{x,l}$, $E_{x,r}$ = electric field within the free space, V m^{-1}
f = frequency of incident radiation, Hz
h = heat-transfer coefficient, W m^{-2} K^{-1}
I_L (I_R) = incident radiation flux from left (right) side, W m^{-2}
k = thermal conductivity of the sample, W m^{-1} K^{-1}
L = half thickness of the sample, m
L_{min} = limiting sample length for thin sample asymptotes, m
L_{R_j} = jth resonating length, m
n = ratio of κ_{mI} and κ_{mR} (see Eq. 22)
p = ratio of κ_0 and κ_{mR} (see Eq. 22)
$q(z')$ = absorbed power distribution within the sample, W m^{-3}
$Q(z)$ = dimensionless absorbed-power distribution within the sample
Q_{avg} = dimensionless average-absorbed power within the sample
T_∞ (T_0) = ambient (initial) temperature, K
z' = spatial coordinate
z = dimensionless spatial coordinate normalized with L

Greek letters

$\delta_{c,j}$ = correction factor for the prediction of jth resonating length
ε_0 = free space permittivity, Farad m^{-1}
ε_R (ε_I) = normalized half sample thickness scaled with $\lambda_m/2\pi(D_{p,m})$ (see Eq. 18)
κ_m = propagation constant within the sample
κ_l, κ_r, κ_0 = propagation constant within the free space
κ_{mR} (κ_{mI}) = real (imaginary) part of κ_m
κ'_m = dielectric constant of the sample
κ''_m = dielectric loss of the sample
λ_i = wavelength within ith medium, m
λ_m = wavelength within the sample, m
ϕ_l (ϕ_r) = fractional incident electric field from left (right) side
ρ = density of the sample, Kg m^{-3}

Literature Cited

Ayappa, K. G., H. T. Davis, G. Crapiste, E. A. Davis, and J. Gordon, "Microwave Heating: An Evaluation of Power Formulations," *Chem. Eng. Sci.,* **46**, 1005 (1991).

Ayappa, K. G., H. T. Davis, E. A. Davis, and J. Gordon, "Two-Dimensional Finite Element Analysis of Microwave Heating," *AIChE J.,* **38**, 1577 (1992).

Ayappa, K. G., H. T. Davis, S. A. Barringer, and E. A. Davis, "Resonant Microwave Power Absorption in Slabs and Cylinders," *AIChE J.,* **43**, 615 (1997).

Ayappa, K. G., "Resonant Microwave Power Absorption in Slabs," *J. Microwave Power and E. M. Energy,* **34**, 33 (1999).

Balanis, C. A. *Advanced Engineering Electromagnetics.* John Wiley and Sons, 1989.

Barringer, S. A., K. G. Ayappa, E. A. Davis, H. T. Davis, and J. Gordon, "Power Absorption During Microwave Heating of Emulsions and Layered Systems," *J. Food. Sci.,* **60**, 1132 (1995).

Basak, T., "Analysis of Resonances During Microwave Thawing of Slabs," *Int. J. Heat Mass Transfer,* **46**, 4279–4301 (2003).

Basak, T., "Role of Resonances on Microwave Heating of Oil-Water Emulsions," *AIChE J.,* **50**, 2659–2675 (2004).

Basak, T., and A. S. Priya, "Role of Ceramic Supports on Microwave Heating of Materials," *J. Appl. Phys.,* **97**, 083537 (2005).

Basak, T., and S. S. Kumaran, "A Generalized Analysis on Material Invariant Characteristics for Microwave Heating of Slabs" *Chem. Eng. Sci.,* **60**, 5480 (2005).

Basak, T., "Generalized Analysis on Microwave-Assisted Material Processing for One-Dimensional Slabs: Metallic Support versus Free Space" *Industrial & Eng. Chem. Res.,* **44**, 3075 (2005).

Ohlsson, T., and P. O. Risman, "Temperature Distribution of Microwave Heating-Spheres and Cylinders," *J. Microwave Power,* **13**, 303 (1978).

Oliveira, M. E. C., and A. S. Franca, "Microwave Heating of Foodstuffs," *J. Food Eng.,* **53**, 347 (2002).

Massoudi, H., C. H. Durney, P. W. Barber, and M. F. Iskander, "Electromagnetic Absorption in Multilayered Cylinder Models of Man," *IEEE Trans. Microwave Theory and Techniques,* **27**, 825 (1979).

Stratton, J. A., *Electromagnetic Theory.* McGraw-Hill Book Company, Inc., 1941.

Weil, C. M., "Absorption Characteristics of Multilayered Sphere Models Exposed to UHF/Microwave Radiation," *IEEE Trans. Biomed. Eng.* **BME-22**, 468 (1975).

Appendix A: Expressions for the Coefficients in Eq. 15

Using

$$\Delta_1 = 2\kappa_{mR}L + (\kappa_{lR} - \kappa_{rR})L, \quad \Delta_2 = 2\kappa_{mR}L - (\kappa_{lR} - \kappa_{rR})L \tag{A1}$$

and

$$\vartheta_1^r = \delta_{lr}^R\delta_{mm}^R, \quad \vartheta_2^r = \delta_{mr}^R\delta_{ll}^R, \quad \vartheta_3^r = \delta_{lm}^R\delta_{rr}^R, \quad \vartheta_4^r = \delta_{ll}^R\delta_{rr}^R \tag{A2a}$$

$$\vartheta_1^i = \delta_{lr}^I\delta_{mm}^R, \quad \vartheta_2^i = \delta_{mr}^I\delta_{ll}^R, \quad \vartheta_3^i = \delta_{lm}^I\delta_{rr}^R \tag{A2b}$$

where δ_{ij}^R and δ_{ij}^I are given by

$$\left.\begin{aligned}\delta_{ij}^R &= \kappa_{iR}\kappa_{jR} + \kappa_{iI}\kappa_{jI}\\ \delta_{ij}^I &= \kappa_{iR}\kappa_{jI} - \kappa_{iI}\kappa_{jR}\end{aligned}\right\}, \quad i, j = l, m, r \tag{A2c}$$

the expressions for c_q's in Eq. 16 a–c can be written as:
Expressions for $c_{q,j}^k$, $k = l, r$, $j = 1$–4

$$c_{q,1}^k = 2e^{2\kappa_{kI}L}\delta_{kk}^R(\delta_{mm}^R - \delta_{jj}^R), \quad c_{q,2}^k = 2e^{2\kappa_{kI}L}\delta_{kk}^R(\delta_{mm}^R + \delta_{jj}^R),$$
$$c_{q,3}^k = 4e^{2\kappa_{kI}L}\delta_{kk}^R\delta_{mj}^I, \; c_{q,4}^k = 4e^{2\kappa_{kI}L}\delta_{kk}^R\delta_{mj}^R, \quad j = \begin{cases} r \text{ for } k = l \\ l \text{ for } k = r \end{cases} \tag{A3}$$

Expressions for $c_{q,j}^{lr}$, $j = 1$–6

$$\begin{aligned} c_{q,1}^{lr} = [&(\vartheta_2^i - \vartheta_1^i - \vartheta_3^i)\sin\Delta_1 + (\vartheta_1^i + \vartheta_2^i - \vartheta_3^i)\sin\Delta_2 \\ &+ (\vartheta_1^r - \vartheta_2^r + \vartheta_3^r - \vartheta_4^r)\cos\Delta_1 \\ &+ (\vartheta_1^r + \vartheta_2^r - \vartheta_3^r - \vartheta_4^r)\cos\Delta_2]e^{\kappa_{lI}L + \kappa_{rI}L} \end{aligned} \tag{A4a}$$

$$\begin{aligned} c_{q,2}^{lr} = [&(\vartheta_2^i - \vartheta_1^i - \vartheta_3^i)\sin\Delta_1 + (\vartheta_3^i - \vartheta_1^i - \vartheta_2^i)\sin\Delta_2 \\ &+ (\vartheta_1^r - \vartheta_2^r + \vartheta_3^r - \vartheta_4^r)\cos\Delta_1 \\ &+ (\vartheta_3^r + \vartheta_4^r - \vartheta_1^r - \vartheta_2^r)\cos\Delta_2]e^{\kappa_{lI}L + \kappa_{rI}L} \end{aligned} \tag{A4b}$$

$$c_{q,3}^{lr} = (\vartheta_1^r + \vartheta_2^r + \vartheta_3^r + \vartheta_4^r)e^{(\kappa_{lI} + \kappa_{rI} + 2\kappa_{mI})L} \tag{A4c}$$

$$c_{q,4}^{lr} = (\vartheta_1^r - \vartheta_2^r - \vartheta_3^r + \vartheta_4^r)e^{(\kappa_{lI} + \kappa_{rI} - 2\kappa_{mI})L} \tag{A4d}$$

$$c_{q,5}^{lr} = -(\vartheta_1^i + \vartheta_2^i + \vartheta_3^i)e^{(\kappa_{lI} + \kappa_{rI} + 2\kappa_{mI})L} \tag{A4e}$$

$$c_{q,6}^{lr} = (\vartheta_1^i - \vartheta_2^i - \vartheta_3^i)e^{(\kappa_{lI}+\kappa_{rI}-2\kappa_{mI})L} \quad \text{(A4f)}$$

Expressions for $c_{q,j}^d$, $j = 1$–4

$$c_{q,1}^d = \frac{1}{2}(\delta_{ll}^R - \delta_{mm}^R)(\delta_{mm}^R - \delta_{rr}^R) + 2\delta_{lm}^I\delta_{rm}^I,$$

$$c_{q,2}^d = \frac{1}{2}(\delta_{ll}^R + \delta_{mm}^R)(\delta_{mm}^R + \delta_{rr}^R) + 2\delta_{lm}^R\delta_{rm}^R,$$

$$c_{q,3}^d = (\delta_{mm}^R - \delta_{ll}^R)\delta_{rm}^I + (\delta_{mm}^R - \delta_{rr}^R)\delta_{lm}^I$$

$$c_{q,4}^d = (\delta_{mm}^R + \delta_{rr}^R)\delta_{lm}^R + (\delta_{ll}^R + \delta_{mm}^R)\delta_{rm}^R \quad \text{(A5)}$$

Appendix B: Expressions for C_0^n, C_0^d, C_1^n, C_2^n, C_1^n, $\eta_{n,1}$, $\eta_{n,2}$, and η_d in Eq. 21

$$C_0^n = \sum_{k=l}^{r}(-4\kappa_{jR}\delta_{kk}^R\delta_{mm}^R e^{2\kappa_{kI}L} + \kappa_{mR}(c_{q,2}^k \sinh 4\kappa_{mI}L + c_{q,4}^k \cosh 4\kappa_{mI}L))\frac{\phi_k^2}{2\kappa_{mI}} \quad \text{(B1a)}$$

$$C_0^d = c_{q,2}^d \cosh 4\kappa_{mI}L + c_{q,4}^d \sinh 4\kappa_{mI}L, \quad \text{(B1b)}$$

$$C_1^d = \frac{1}{2}\sqrt{((\delta_{mm}^R + \delta_{rr}^R)^2 - 4(\delta_{mr}^R)^2)((\delta_{mm}^R + \delta_{ll}^R)^2 - 4(\delta_{ml}^R)^2)} \quad \text{(B1c)}$$

$$C_1^n = 2\phi_l\phi_r\sqrt{\left(\sum_{k=1}^{2}\ell_{k1}\cos\gamma + \sum_{k=1}^{2}\ell_{k2}\sin\gamma\right)^2 + (\ell_{31}\cos\gamma + \ell_{32}\sin\gamma)^2}, \quad \gamma = (\kappa_{lR} - \kappa_{rR})L \quad \text{(B1d)}$$

$$C_2^n = \sqrt{4\left(\sum_{k=l}^{r}\delta_{kk}^R\delta_{mj}^I\phi_k^2 e^{2\kappa_{kI}L}\right)^2 + \left(\sum_{k=l}^{r}\delta_{kk}^R(\delta_{mm}^R - \delta_{jj}^R)\phi_k^2 e^{2\kappa_{kI}L}\right)^2} \quad \text{(B1e)}$$

$$\eta_{n,1} = \text{sign}(\ell_{31}\cos\gamma + \ell_{32}\sin\gamma)\cos^{-1} \times \frac{2\phi_l\phi_r\sum_{k=1}^{2}(\ell_{k1}\cos\gamma + \ell_{k2}\sin\gamma)}{C_1^n} \quad \text{(B1f)}$$

$$\eta_{n,2} = \text{sign}(\phi_l^2 c_{q,3}^l + \phi_r^2 c_{q,3}^r)\cos^{-1}\frac{\phi_l^2 c_{q,1}^l + \phi_r^2 c_{q,1}^r}{2C_2^n} \quad \text{(B1g)}$$

$$\eta_d = \text{sign}(c_{q,1}^d)\cos^{-1}\frac{c_{q,3}^d}{C_1^{Q,d}} \quad \text{(B1h)}$$

where

$$\ell_{11} = \frac{2\delta_{mm}^R}{\kappa_{mI}}(\delta_{ll}^R\kappa_{rI} + \delta_{rr}^R\kappa_{lI})\sinh(2\kappa_{mI}L)e^{\kappa_{lI}L+\kappa_{rI}L}, \quad \text{(B2a)}$$

$$\ell_{12} = \frac{2\delta_{mm}^R}{\kappa_{mI}}(\delta_{ll}^R\kappa_{rR} - \delta_{rr}^R\kappa_{lR})\sinh(2\kappa_{mI}L)e^{\kappa_{lI}L+\kappa_{rI}L}, \quad \text{(B2b)}$$

$$\ell_{21} = 2(\delta_{mm}^R\delta_{lr}^R + \delta_{rr}^R\delta_{ll}^R)\cosh(2\kappa_{mI}L)e^{\kappa_{lI}L+\kappa_{rI}L}, \quad \text{(B2c)}$$

$$\ell_{22} = 2\delta_{mm}^R\delta_{rl}^I\cosh(2\kappa_{mI}L)e^{\kappa_{lI}L+\kappa_{rI}L}, \quad \text{(B2d)}$$

$$\ell_{31} = \frac{2\kappa_{mR}}{\kappa_{mI}}(\delta_{mm}^R\delta_{lr}^R - \delta_{rr}^R\delta_{ll}^R)\sinh(2\kappa_{mI}L)e^{\kappa_{lI}L+\kappa_{rI}L}, \quad \text{(B2e)}$$

$$\ell_{32} = \frac{2\kappa_{mR}}{\kappa_{mI}}\delta_{mm}^R\delta_{rl}^I\sinh(2\kappa_{mI}L)e^{\kappa_{lI}L+\kappa_{rI}L} \quad \text{(B2f)}$$

and

$$j = \begin{cases} r \text{ for } k = l \\ l \text{ for } k = r \end{cases}$$

Above expressions can be simplified for $\kappa_{lR} = \kappa_{rR} = \kappa_0$ and $\kappa_{lI} = \kappa_{rI} = 0$ as

$$C_0^n = \frac{(\phi_l^2 + \phi_r^2)p^2}{n}[(1 + n^2 + p^2)\sinh 4\varepsilon_I + 4p\sinh^2 2\varepsilon_I - 2n^2 p] \quad \text{(B3a)}$$

$$C_1^n = \frac{4\phi_l\phi_r p^2}{n}[n^2(1 + n^2 + p^2)^2\cosh^2 2\varepsilon_I + (1 + n^2 - p^2)^2\sinh^2 2\varepsilon_I]^{1/2} \quad \text{(B3b)}$$

$$C_2^n = (\phi_l^2 + \phi_r^2)p^2\sqrt{(1 + n^2 - p^2)^2 + 4n^2p^2}, \quad \text{(B3c)}$$

$$C_0^d = \frac{1}{2}(((1 + n^2 + p^2)^2 + 4p^2)\cosh 4\varepsilon_I + 4p(1 + n^2 + p^2)\sinh 4\varepsilon_I) \quad \text{(B3d)}$$

$$C_1^d = \frac{1}{2}((1 + n^2 - p^2)^2 + 4n^2p^2) \quad \text{(B3e)}$$

$$\eta_{n,1} = \text{sign}(1 + n^2 - p^2)\cos^{-1} \times \frac{n(1 + n^2 + p^2)}{\sqrt{n^2(1 + n^2 + p^2)^2 + (1 + n^2 - p^2)^2\tanh^2 2\varepsilon_I}} \quad \text{(B3f)}$$

$$\eta_{n,2} = -\cos^{-1}\frac{1 + n^2 - p^2}{\sqrt{(1 + n^2 - p^2)^2 + 4n^2p^2}} \quad \text{(B3g)}$$

$$\eta_d = \text{sign}(4n^2p^2 - (1 + n^2 - p^2)^2)\cos^{-1} \times \frac{4np(1 + n^2 - p^2)}{(1 + n^2 - p^2)^2 + 4n^2p^2} \quad \text{(B3h)}$$

where $p = \kappa_{mR}/\kappa_0$ and $n = \kappa_{mR}/\kappa_{mI}$.

Appendix C: Coefficients $c^{\delta}_{j,1}$, $c^{\delta}_{j,2}$, and $c^{\delta}_{j,3}$ in Eq. 24b

$$c^{\delta}_{j,1} = 2\frac{\psi_1}{\psi_d} - \frac{\left(\frac{d(LC^d_0)}{dL}(C^n_0 + 4\ell_2\phi_l\phi_r)\right)_{L=L_{c,j}}}{\psi^2_d} \quad \text{(C1a)}$$

$$c^{\delta}_{j,2} = -2\left(\frac{c^{\delta}_{j,1}}{\psi_d}\frac{d(LC^d_0)}{dL} + \frac{(C^n_0 + 4\phi_l\phi_r\ell_2)\left(\frac{dC^d_0}{d\varepsilon_R} + 8n\kappa_{mI}LC^d_0\right)}{\psi^2_d}\right)_{L=L_{c,j}} + 2\frac{\psi_2}{\psi_d} \quad \text{(C1b)}$$

$$c^{\delta}_{j,3} = -\left[\frac{1}{\psi_d}\frac{d(LC^d_0)}{dL}\left(\frac{d(LC^d_0)}{dL}\frac{c^{\delta}_{j,1}}{\psi_d} + 2c^{\delta}_{j,2} - \frac{\psi_2}{\psi_d}\right) + 2\frac{\frac{dC^d_0}{d\varepsilon_R} + \frac{8nL}{D_{p,m}}C^d_0}{\psi_d}\left(c^{\delta}_{j,1} + \frac{\psi_1}{\psi_d}\right)\right]_{L=L_{c,j}} + 8n^2\left(c^{\delta}_{j,1} - 2\frac{C^d_0(C^n_0 + 4\ell_2\phi_l\phi_r)}{\psi^2_d}\right)_{L=L_{c,j}} + 16\frac{(\ell_1 - 3n\ell_2\tanh 2\kappa_{mI}L_{c,j})(1+n^2)\phi_l\phi_r}{\psi_d}, \quad \text{(C1c)}$$

where

$$\psi_1 = (\phi^2_l + \phi^2_r)(c^0_{q,2}\cosh 4\kappa_{mI}L_{c,j} + c^0_{q,4}\sinh 4\kappa_{mI}L_{c,j}) + 4\phi_l\phi_r(n\ell_2\tanh 2\kappa_{mI}L_{c,j} - \ell_1) \quad \text{(C2a)}$$

$$\psi_2 = 4n(\phi^2_l + \phi^2_r)(c^0_{q,4}\cosh 4\kappa_{mI}L_{c,j} + c^0_{q,2}\sinh 4\kappa_{mI}L_{c,j}) - 8\phi_l\phi_r(\ell_2(1-n^2) + 2n\ell_1\coth 2\kappa_{mI}L_{c,j}) \quad \text{(C2b)}$$

$$\psi_d = \kappa_{mR}L_{c,j}C^d_0|_{L=L_{c,j}} \quad \text{(C2c)}$$

$$\ell_1 = \frac{p^2(1+n^2-p^2)}{n}\sinh 2\kappa_{mI}L_{c,j}, \quad \text{(C2d)}$$

$$\ell_2 = p^2(1+n^2+p^2)\cosh 2\kappa_{mI}L_{c,j}, \quad \text{(C2e)}$$

and

$$\frac{2L_{c,j}}{\lambda_m} = \frac{4j+1}{4}, \quad j = 1, 2, 3 \ldots \quad \text{(C2f)}$$

In the earlier equations, ε_R and ε_I are given in Eqs. 18, $c^0_{q,j}$ is same as $c^l_{q,j}$ or $c^r_{q,j}$ in Appendix A with $\kappa_{lR} = \kappa_{rR} = p\kappa_{mR}$, $\kappa_{lI} = \kappa_{rI} = 0$ and $\kappa_{mI} = n\kappa_{mR}$, while C^d_0 and C^n_0 are given in Eqs. B3d and 3a, respectively (see Appendix B).

Appendix D: Coefficients a_j, b_j, and τ_j in Eq. 32

$$a_1 = \frac{4}{3}(n^2 + p^2 - 1 - p^2\phi_l\phi_r) \quad \text{(D1a)}$$

$$a_2 = \frac{8}{3}(\phi^2_l + \phi^2_r)np \quad \text{(D1b)}$$

$$a_3 = \frac{4}{15}(4(1 + n^4 - p^2 + n^2p^2) + (6p^2(1-n^2) - 5(1+n^2)^2)\phi_l\phi_r) \quad \text{(D1c)}$$

$$b_1 = 4\frac{n}{p} \quad \text{(D1d)}$$

$$b_2 = \frac{(n^2+p^2-1)^2 + 4n^2}{p^2} \quad \text{(D1e)}$$

$$b_3 = \frac{16n}{3p}(n^2+p^2-1) \quad \text{(D1f)}$$

$$b_4 = \frac{\frac{4}{3}(n^2(1+n^2+p^2)^2 - (1+n^2-p^2)^2)}{p^2} \quad \text{(D1g)}$$

$$\tau_0 = -180np \quad \text{(D2a)}$$

$$\tau_1 = -30(3(1+n^2)^2 - 2p^2(1-n^2) - p^4(1 - 4\phi_l\phi_r)) \quad \text{(D2b)}$$

$$\tau_2 = -120np(-4(1-n^2) + p^2(1 + 8\phi_l\phi_r)) \quad \text{(D2c)}$$

$$\tau_3 = -48(-(5(1+n^2)^2 + p^4)(1-n^2) + 6(1+n^4)p^2 + (5(1 + 10n^2 + n^4)p^2 - 6(1-n^2)p^4)\phi_l\phi_r) \quad \text{(D2d)}$$

$$\tau_4 = 8np(47(1+n^2)^2 - 22p^2(1-n^2) + 16n^2 - 25p^4 - 2(60(1+n^2)^2 - 64p^2(1-n^2) - 5p^4)\phi_l\phi_r) \quad \text{(D2e)}$$

$$\tau_5 = -8(8(n^4(n^4 - 8 + 3p^2(3+p^2)) - (n^2(3(1+n^4) + p^2(12+p^2)) - (1-p^2)^2)(1-p^2)) + ((1+n^2)^2(15(1+n^2)^2 - 28(1-n^2)p^2) + (11-n^2)(1-11n^2)p^4 + 2(1-n^2)p^6)\phi_l\phi_r)$$

$$\tau_6 = 32np(-3(1-n^6) + (13n^2 - 3p^4 + 6p^2(1-n^2))(1-n^2) - 24n^2p^2 - 2p^2((1-n^2)^2 - p^2 + n^2(-20+p^2))\phi_l\phi_r) \quad \text{(D2f)}$$

Manuscript received Jan. 30, 2006, and revision received July 12, 2006.